53)

Velocity fluctuations in slow flow through porous media

by

Olav van Genabeek

M.Sc., Harvard University (1992)

Submitted to the Earth, Atmospheric and Planetary Sciences
in partial fulfillment of the requirements for the degree of

Doctor of Philosophy

at the

MASSACHUSETTS INSTITUTE OF TECHNOLOGY

~~July 1998~~
[September 1998]

Author ....
Earth, Atmospheric and Planetary Sciences
July, 1998

Certified by ....
Daniel H. Rothman
Professor, MIT
Thesis Supervisor

Accepted by ....
Ronald G. Prinn
Department Head, Deparment of Earth, Atmospheric, and Planetary Sciences

Velocity fluctuations in slow flow through porous media

by

Olav van Genabeek

Submitted to the Earth, Atmospheric and Planetary Sciences
on July, 1998, in partial fulfillment of the
requirements for the degree of
Doctor of Philosophy

Abstract

In this thesis, I study the spatial statistical properties of slow flow through porous media on the pore scale by a combination of numerical simulation and theoretical arguments. I demonstrate that the flow patterns undergo a transition from swirls to strongly focused and channel-like patterns for decreasing porosities. Not only is the flow in low-porosity media strongly focused, but the flow also possesses long-tailed, non-Gaussian velocity probability density distributions. A main result of our simulations is that the statistics of the flow through a single channel captures the entire flow, insofar as the patterns and probability distributions are concerned. I have constructed a simplified, phenomenological model for the fast part of the flow in random porous media. This model yields the desired exponential velocity distributions. For high porosities, I find that the statistical properties of the velocity fluctuations behave in a similar way as those observed in dilute suspensions flows: the swirls have a power-law dependency on the solid volume fraction, the correlation length is finite and has also a power-law dependency. I demonstrate that this scaling behavior is consistent with the predictions of theories. Finally, I study creeping flow through a single rough walled channel by numerical simulation and present a theory that predicts scale dependency of the permeability for tight fractures.

Thesis Supervisor: Daniel H. Rothman
Title: Professor, MIT

Acknowledgments

I dedicate this thesis to my parents, Gerard van Genabeek and Mechtilda Krijn, whom I have loved so much. Regrettably, they both have passed away a while ago.

Without my best friend and wife Amy, this thesis would never have been written. I want to thank her for all her support and the love she have given me during these years. She has been coping with a lot from me (not that she won't have to put up with a lot once we are leaving Cambridge), and I thank her for that too. Furthermore she has given me three wonderful sons, Maarten and Noah and Seth, who are giving me the most joy in my life. Thanks guys, without you, life would be much and much less fun. I thank my mother in law Anne Kantor for all she did for me, which is substantial.

I thank Dan for being a great supervisor and I am grateful to the opportunity to work with and to know him. Dan gave me total freedom early on during my academic career. Nevertheless, he was always more than happy to guide and help me.

In the spring of 1994, I visited the department, initially for a recommendation of Tom Jordan. At that time I was not thinking of applying to EAPS at all. I was planning to apply for the Mathematics department at MIT instead. Tom Jordan convinced me to talk to Dan, since he thought correctly that I would be interested to work with. What a great choice it turned out to be! I thank Tom Jordan very much for this.

I am indebted to Michael Brenner. Michael has been the great other advisor during the final stage of my research. He helped me to develop the "leaky channel" model which I consider as the core of my research.

A selfish undertaking such as this cannot be done without the support of many friends. In particular, I would like to thank Peter Dodds. Peter has been a great friend. Peter, a crazy Australian, really tried hard (unsuccessfully though) to get me involved in sports.

It has been a true joy to meet Romualdo Pastor-Satorras, whom I deeply respect. I have learned a lot from him.

It has also been a great honor to have John Bush as a friend. I met John during my Harvard years. John went off to Cambridge pursuing a brilliant career. I feel very lucky to know John, not only as a scientist, but also as a person.

Without the help of Terri Macloon and Jane Shapiro, I would have never gotten anything done. It has been great to know you and I truly appreciate your help.

In no particular order, I thank Alessandro Forte, Kelvin Chan, Clint Conrad, Rafi Katzman, John Olson, and Einat Aharanov.

Contents

Chapter 1

Introduction

Recent advances in computational physics allow for the numerical simulation of three-dimensional complex flows through arbitrarily complex geometries. Moreover, new technology for non-invasive imaging has provided detailed three-dimensional tomographic reconstructions of porous rocks with resolution approaching one micron. These two innovations are leading to a new understanding of how the microscopic complexity of natural porous media influences fluid transport at a macroscopic scale. Because of the complexity of the underlying porous structure, the flow is highly disordered. This disorder gives rise to spatial velocity fluctuations, which form the principal topic of research in this thesis. Simply stated, the goal of this thesis is to obtain new insights into slow flow through complex structures by numerical modeling the microscopic details of the flow and developing supporting theoretical arguments.

In an average sense, flow through porous media is well understood since the observations of Darcy [8] in the 19th century. Darcy's law states that the flow rate is given by a constant, known as the permeability, times the external pressure gradient. Despite its success, Darcy's law does not provide any insight other than the behavior of average properties. Consequently, porous media with different geometries can still yield the same transport properties, such as the permeability.

There are many practical concerns ranging from contaminant migration in groundwater to the efficiency of oil recovery, where one would like to be able to predict the permeability from the statistical properties of the porous geometry. Indeed, in the past, many attempts [8, 53, 2] have been made to relate the permeability k to statistical properties of the media. Most of these efforts, however, have been on simplified and essentially macroscopic models for the media, such as capillary models [53]. Then, by introducing enough degrees of freedom, satisfactory fits can be found for the permeability. While these models have been highly effective, there is, however, little physical evidence for such models. I pursue a fundamentally different approach. Instead, I use the observations of the microscopic flow field themselves to construct models of the flow. These models are at scales larger than the pore scale, but smaller than the Darcy scale. Therefore, my models are intended as a simplification of the Stokes equations for fluid flow inside the pores. They do provide, however, more details of the flow than Darcy's equation.

In this thesis, flow through two distinct types of porous media has been studied by numerical simulations of Stokes flow. These are, namely, random porous media and rough-walled channels (fractures). Common to both media is that the flow is conditioned by the porosity or average channel height. They differ in that the flow in channels is much more strongly correlated. In any case, they constitute an important part of the large set of possible porous media.

In contrast to common beliefs, flow through random porous media has a very rich phenomenology. To make this point clear, consider the conditioning of the flow in random porous media by the porosity. In figure 1-1 the intensity of the flow speed for a multitude of porosities is displayed for a 2D random media. At low porosity the fast part of the flow is strongly focussed and localized in a strong branching network of channels, whereas at larger porosities this channel-like pattern has completely disappeared. Because of the richness in phenomenology, I have considered each end of the porosity spectrum separately.

Flow through a rough walled channel is another principal form of fluid transport, particularly in sedimentary basins. The complexity in the flow is due to the complexity or roughness of its channel wall. It should be no surprise that the effects on the complexity of the flow increases when the two opposite fracture walls are approaching each other. In this thesis, I will show that for the case that the fracture is almost

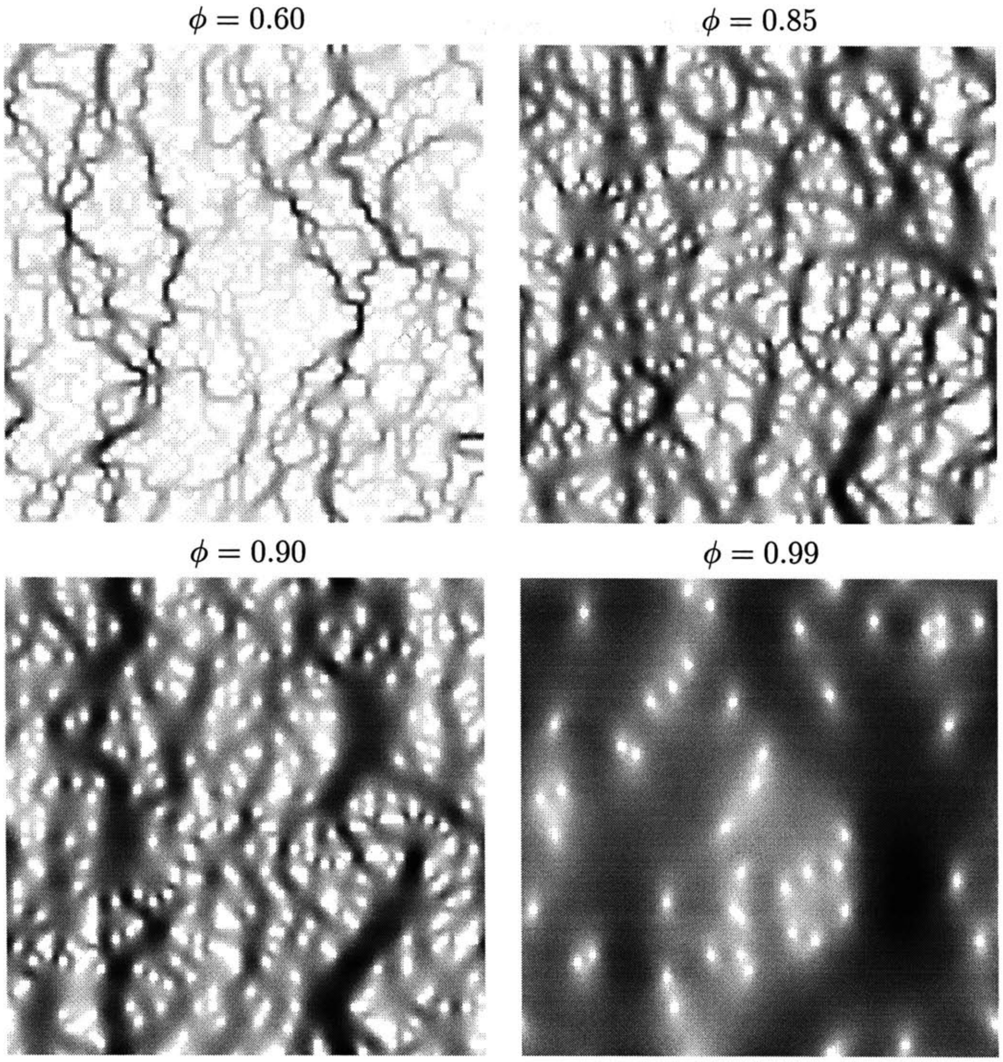

$\phi = 0.60$ $\phi = 0.85$

$\phi = 0.90$ $\phi = 0.99$

Figure 1-1: Intensity plots of the relative speed $|\mathbf{u} - \bar{\mathbf{u}}|$ for different values of the porosity ϕ. The fastest velocities are in black. Note, that the channel-like pattern becomes apparent for porosities $\phi < 0.85$.

closed, the permeability can be related to statistical properties of the walls in a natural way. This is one of the rare occasions that the transport properties of flow can be coupled to the geometry of the channel walls.

In the first part of this thesis (Chapter II) I study flow in porous media with low porosity, such that the fast part of the flow is organized in channel-like structures. I construct a physical model in which the porous media is simplified to a single channel with leaky walls. With this model I am able to explain much of the observed flow phenomenology, such as the exponential tails in the velocity distributions. The porous media studied in Chapter III are essentially the same as the primary porous structures studied in Chapter II, but have a much larger porosity. The fluctuations in the velocity field at high porosities are in the form of swirls. The phenomenology of these swirls is very similar to the phenomenology observed in the fluctuations of the particle velocities in sedimenting suspensions. In this chapter, I will propose a simple argument for the size of the swirls.

Next, Chapter IV, I study flow through a fracture model. In this model, the fracture is the void space between two juxtaposed fractal channel walls. The functional dependence of the permeability with the average channel height is carefully determined. For a tight fracture, I derive a scaling relation for the permeability as a function of the length of the fracture. This derivation is based on percolation arguments of fractal surfaces.

Chapter 2

Velocity fluctuations in slow flow through porous media

Abstract

We study the spatial velocity fluctuations in slow flow through porous media at the pore scale by numerical simulation of Stokes equations and theoretical arguments. The numerical simulations show that the flow in low-porosity media is strongly focused into channelized structures. These localized flow patterns result in long-tailed, stretched exponential probability density functions (PDF's) for the velocity. The simulations show that for increasing values of the porosity the channel-like patterns disappear and become swirls, characterized by Gaussian fluctuations. Computation of fourth moments of the velocity field show that this transition is sharp. The exponential decay in the velocity distribution for low porosities, which has also been observed in previous studies, appears to be a generic property of flow through complex low-porosity porous structures. Numerical simulations show that the velocity fluctuations in individual flow paths in such flows are also described by the same PDF. Motivated by these findings, we construct a theoretical model in which the porous medium is simplified to a single channel with leaky walls, that allows the fluid to both enter and leave the channel. With this theory the statistics of the branching of the individual channel can be characterized and the stretched exponential tails in the velocity distribution can be explained.

2.1 Introduction

Complex flows often require a statistical description. For example, in studies of hydrodynamic turbulence, statistical correlations and histograms of fluctuations have played a long and illustrious role [5, 37, 22]. The study of sedimenting suspensions is another example where statistical characterizations of the velocity field and the fluid particle interactions have proven useful [7].

One might naively assume that steady slow laminar flow would never require such an approach. However, when the flow occurs through complex geometries such as microscopically disordered porous media, the spatial fluctuations of velocity attain a considerable complexity. As with other complex flows, certain questions of a statistical nature arise naturally. How can the velocity fluctuations be characterized? What are their correlations? How do these vary as a function of the relevant control parameter? Can a simple physical model be constructed that captures these phenomena, thus offering fundamental insight into their origin? These are new questions in the context of flow through porous media, and the purpose of this chapter is to address them.

The correct macroscopic transport equation for flow through porous media has been known since the last century. Known as Darcy's law [8], it can be written as

$$Q = \frac{k}{\mu}\nabla P, \tag{2.1}$$

where Q is the average flux through unit area per unit time, k is the permeability and ∇P is the applied external pressure gradient. To date, most work on flow through porous media has concentrated on relating bulk transport properties, such as the permeability, to bulk geometric properties of the media, such as the porosity (i.e., the void fraction) [53, 8, 2].

Although such approaches have met with some success, it is not uncommon for them to make grossly erroneous predictions. The reason for this may be simply understood. A "perfect" prediction of permeability would require solving the Stokes equations in a highly complex geometry. Theories that attempt to relate permeability to porosity, on the other hand, in essence attempt to project both the flow and the geometry on their first statistical moments. Thus it is clear that if a model could be constructed that included higher-order statistics, its predictions would be closer to reality. Indeed, this observation is not new, and it has been exploited in the past to derive variational bounds on the permeability [42, 65, 11, 48].

In recent years another approach to flow through porous media, based on numerical simulation, has been developed [63]. Here one really does solve the Stokes equations in a complex geometry. The geometry may be as complex as one desires: simulations have been reported in media as diverse as sphere packs [17, 33, 36]), fractal geometries [34], digital images of real sedimentary rocks [59, 58, 16, 21, 39] and clay [26], models of fiber webs [30], and random 2D media [3]. While in this manner one may arguably obtain the aforementioned perfect prediction, direct numerical simulation of the Stokes equation does not in and of itself yield fundamental insight. However, because such simulations solve for the flow field everywhere within the pore space, they do in principle provide the information necessary for obtaining a more sophisticated characterization of the flow.

Here we employ numerical simulation of the Stokes equation and attempt to extract as much information as we can from the microscopic pore-scale velocity fields. Whereas the ultimate objective of this approach would include a better prediction of bulk transport, the goal of this chapter is different. Specifically, we seek a new representation of porous flow that is intermediate between the voluminous detail obtained from solutions of the Stokes equation and the simple average represented by Darcy's law. In this way we hope that our work may help pave the way towards further progress in studies of bulk transport properties.

To achieve this objective, we first note that for decreasing values of the porosity the fast part of the flow fluctuations becomes strongly localized into channel-like structures, whereas for large porosities the fluctuations are in the form of swirls. The fluctuations of the slow part of the flow at low porosities has recently been studied by [3] They find that the low-porosity flow is power-law distributed. In this chapter, however, we concentrate on the velocity fluctuations of the fast part of the flow. As we show, this is the portion of the velocity field that forms the channelized structures.

To characterize the lower-porosity flow, our approach is to use the computed velocity fields to find the paths $p_i(\tau)$ that the ith tracer particle would take to traverse the medium, with τ the distance or time along the path. We define these paths to lie within effective channel walls that are separated by a width $h_i(\tau)$ that can itself be defined from the velocity field. The channel walls can leak fluid in and out; consequently, the average velocity $\hat{u}_i(\tau)$ and the flux $\psi_i(\tau) = h_i(\tau)\hat{u}_i(\tau)$ vary with τ.

We study the fluctuations of the channel properties h, $\hat{u}$ and ψ. Our principal results concern their probability density distributions PDF's. For large values of the fluctuating quantity, each of these PDF's may be described by exponentially decaying histograms when the porous medium is of sufficiently low porosity. The case of $\hat{u}$ is of particular interest, because previous laboratory studies [33, 31] and numerical simulations [33, 39, 36] have found exponential tails in histograms of velocity fields $u(\mathbf{x})$ obtained throughout the entire flow field. This observation is fundamental. A naive guess would predict Gaussian PDF's for the fluctuations of u. As we show, the exponential tails are the signature of a kind of spatial intermittency which is induced by the focusing of the flow into the channels. We argue that any one of the channels is representative of the entire medium insofar as the tails of the velocity histograms are concerned. Motivated by our channel construction, we construct a fluctuating channel-flow equation that predicts these exponential PDF's, and thus the exponentially decaying probabilities of the entire velocity field itself.

This chapter is organized as follows. First, we briefly describe the numerical method we have employed for the solution of Stokes equation, followed by an equally brief discussion of the porous medium models used in our studies. Next, we show that for sufficiently low porosities, both two-dimensional and three-dimensional porous structures yield exponential PDF's for the velocity fields. We thus concentrate our attention in the remainder of the chapter on two-dimensional media, which allows us to study systems of much larger linear dimension and correspondingly longer flow paths. We show that the flow fluctuations take the form of channelized structures only for sufficient low porosities, and that this channelized regime is separated sharply from a high-porosity regime of swirls. Then, we detail the extraction of the channels from the low-porosity simulation data, and include a detailed test of the consistency of its statistics. We describe the fluctuations and the correlations of the channel properties along the flow path, and show which of these are representative of the fluctuations of flow through the entire medium. We then present our theoretical model of flow through a single leaky channel. This theoretical model leads to a stochastic differential equation with multiplicative noise, from which we derive the stretched exponential tails. Our model is unusual in that a single leaky channel serves as a simplified model for the connectivity of the entire porous structure. In this way, we provide an attractive alternative to the more conventional parallel tube models of porous flow [8, 53].

2.2 Numerical procedure

To simulate fluid flow, we have employed the Lattice Boltzmann method, which derives from discrete lattice-gas cellular automata [46]. The lattice Boltzmann method solves numerically the incompressible Navier Stokes equations with no-slip boundary conditions at the solid fluid boundaries. Specifically, it solves

$$\begin{aligned} \rho\left(\partial_t \mathbf{u} + \mathbf{u}\cdot\nabla\mathbf{u}\right) &= \mu\nabla^2\mathbf{u} - \nabla p && (2.2)\\ \nabla\cdot\mathbf{u} &= 0 && (2.3)\\ \mathbf{u}|_{\partial V} &= 0, && (2.4) \end{aligned}$$

where $\mathbf{u}$ is the velocity, p is the pressure, ρ is the density, μ is the viscosity, V is the pore space and ∂V is the solid fluid boundary. In our version of the lattice Boltzmann method the no slip boundary condition is implemented using the bounceback method [20]. We apply periodic boundary conditions in all our simulations.

Other numerical methods could have been used, such as finite difference techniques [40], to solve the Navier-Stokes equations. We have chosen the lattice Boltzmann method because, as with lattice-gases, it is easy to implement for problems of low Reynolds number flow through complex geometries [45, 32, 21, 26, 36, 30]. The particular lattice Boltzmann schemes we have employed in this study are an eighteen velocity model for three dimensional flow and a nine velocity model for two dimensional flow [43].

In general, away from the solid-fluid boundaries, the accuracy of the lattice Boltzmann method is second order in the lattice spacing. Near the solid-fluid boundaries the lattice Boltzmann methods are less accurate, with the accuracy depending strongly on the implementation of the boundary conditions. Optimized implementations of the Boltzmann method near the boundaries are discussed by Ginzbourg et al. [23, 24]. With their recipe an accuracy close to second order can be achieved. Naturally, small pores are less resolved and therefore the flow is less accurately simulated in those pores. We performed simulations to investigate the effects of the grid size on the flow. These studies showed that the flows converged when the pore opening contained four or more lattice sites. Nevertheless, to further minimize any possible errors, our most crucial simulations (detailed in section 2.5) were performed with a minimum pore size of eight lattice sites across. Furthermore, since the fastest flow occurs in the larger pores which are th best resolved, it is unlikely that the inaccuracy due to the smaller pores has a strong impact on the tails of the probability distributions.

2.3 Patterns and fluctuations in model porous media

We have performed flow simulations for both 2D and 3D media. In this section, we show that, insofar as the flow patterns and the velocity PDF's are concerned, the flow in both 2D and 3D behaves in a similar way. The similarity is useful for us, because we will later specialize to two dimensional studies.

2.3.1 Geometry

We discuss three different porous structures: a 3D random closed-packed assembly of hard spheres [56, 1], a 3D microtomographic image of Fontainebleau sandstone [4, 39], and a 2D random medium. Figure 2-1 illustrates the three media.

The porosity of the random closed packed mono-dispersed sphere assembly is 36%.

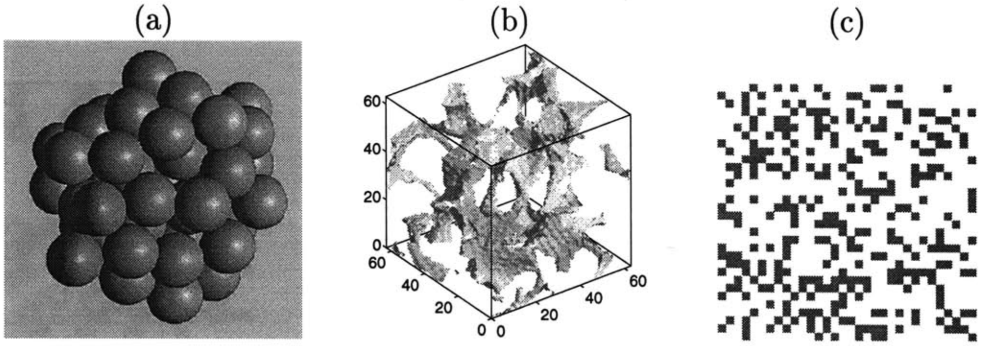

Figure 2-1: Models of porous media. A portion of a random closed-packed assembly of spheres (a) and a tomographic reconstruction of Fontainebleau sandstone (b). In the latter case, the pore-void interface is shown in gray, and the linear dimension is about 0.5 mm. A random two dimensional porous media with porosity $\phi = 0.68$ is depicted in (c). The solid square shaped grains are shown in gray.

The simulations of flow through it are performed on a cubic sample with a side length of 64 nodes. The radius R of each sphere is 6 nodes; thus each side of the cube fits about six sphere diameters.

The sample of Fontainebleau sandstone in our simulations consists of 64^3 cubic cells or voxels. Each voxel has a linear size of $7.5\mu m$ and is mapped on to a lattice node. Hence, the sample cube shown here has a linear dimension of 0.48mm. The porosity of this particular sample is 9.2%.

The 2D media are constructed on a square lattice. A random number p is assigned to each site of this lattice. If the value p at a site is less than a fixed value $\phi < 1$, then the site is identified as a solid side. Hence, ϕ is equal to the porosity of the medium. To insure that the particles do not overlap and that a minimal separation d (in lattice nodes) exists between the grains, the assignment of the solids sites was performed on a coarse grained lattice containing L^2/d^2 lattice nodes. Note that each solid site in the coarse grained lattice corresponds to a square shaped grain with a length of d lattice nodes in the original lattice.

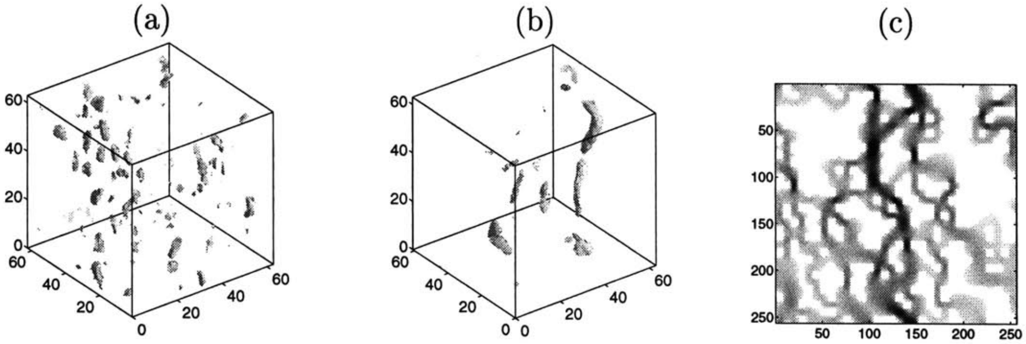

Figure 2-2: Locations of the fastest flow through the three porous media shown in figure 2-1. In all three pannels the main flow is in the vertical direction. In (a) flow through a random sphere pack, and (b) flow through Fontainebleau sandstone the surfaces contain the locations of the fastest 0.4% and 0.3% of the component of the pore velocity in the forcing (vertical) direction. Panel (c) is an intensity of plot of the $u = |\mathbf{u}|$ in the 2D random medium. Here, the fastest velocities are black. In all three cases it is clearly observable that the fastest part of the flow is localized into channel-like structures.

2.3.2 Patterns and velocity histograms

Figure 2-2 shows the locations of the fastest flow through the three different structures of figure 2-1. Note that the regions of the fastest flow are spatially concentrated, or focused, especially in the case of the sandstone and the 2D random medium.

As a result of this focusing, a histogram of the flow velocities in the pore space should contain long (non-Gaussian) tails that reflect the the importance of extreme values in the velocity distribution. Figure 2-3 shows the resulting histograms for our three media. The straight lines in both figures 2-3a), and 2-3b) are least-squares fits to the form

$$P_u(u/\bar{u}) \propto \exp\left[-\beta u/\bar{u}\right], \tag{2.5}$$

where u is the component of the pore velocity in the forcing direction for the case of the 3D media and $u = |\mathbf{u}|$ for the case of the 2D medium. The fits are made to fastest velocities. We find $\beta = 1.3 \pm 0.03$ for the packed sphere model, which is in good agreement with the experimental results of Lebon et al. [33]. The exponential fit for the Fontainebleau sandstone gives a similar decay rate, $\beta = 1.1 \pm 0.05$. On the

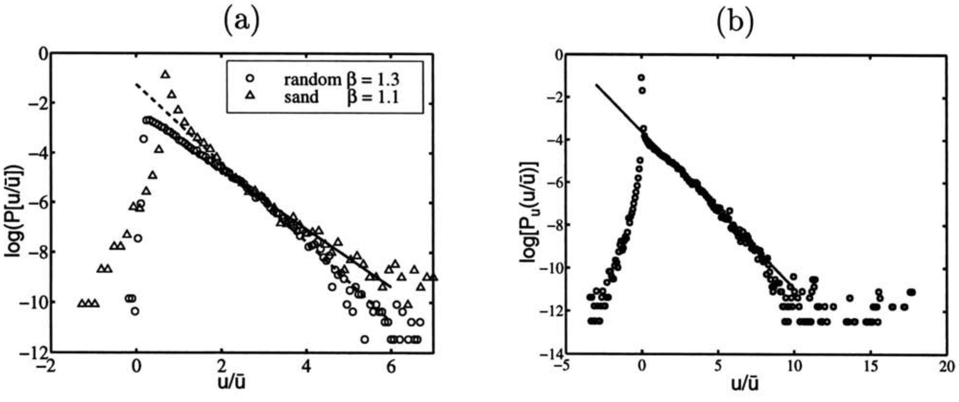

Figure 2-3: Velocity PDF's for the three flows of figure 2-2. (a) PDF's of the velocity component in the main flow direction for flow through bead-packs (circles) and sandstone (triangles), respectively. (b) PDF of $|\mathbf{u}|$ for 2D random medium.

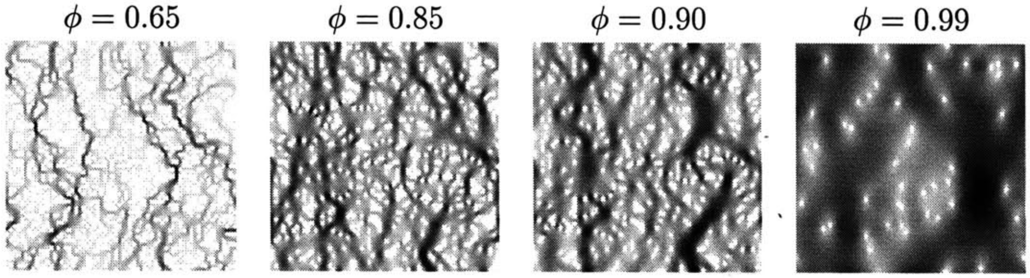

Figure 2-4: Intensity plots of $|\mathbf{u} - \bar{\mathbf{u}}|$ for different values of ϕ. The main flow is in the vertical direction. The fastest velocities are black. Note that channel-like patterns are clearly observable for low porosities.

other hand, the random 2D model yields $\beta \simeq 0.7$.

In summary, we find that, insofar as spatial patterns and the form of PDF's of velocity are concerned, flow through two and three dimensional is similar. Thus, in the remainder of the chapter we limit the discussion to 2D media.

2.4 Porosity dependence of fluctuations: Transition from channels to swirls

The velocity fluctuations are strongly conditioned by the porosity. Several striking effects of this porosity dependence can be observed. First, as seen in figure 2-4, a channel-like pattern becomes apparent for sufficiently small porosities. The organiza-

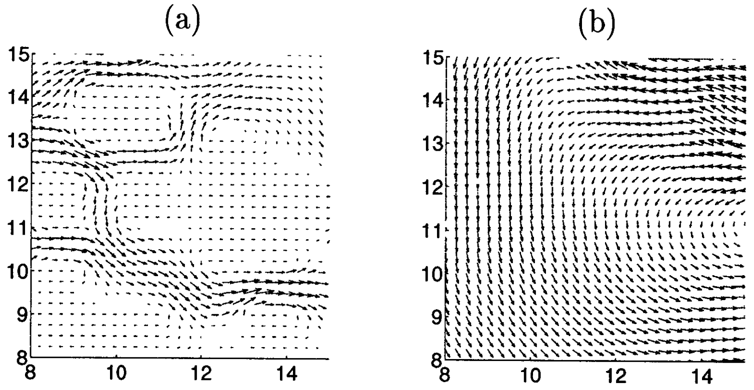

Figure 2-5: Vector velocity maps for part of the flow fields. (a) Partial map for flow through a 2D random medium with $\phi = 0.65$. (b) Partial map for a random medium with $\phi = 0.98$. Here the flow takes the form of swirls. The axis labels are in units of the grain size d and the main flow direction is from left to right.

tion of flow into channels is understandable for very small porosities, since close to the percolation threshold of the porous medium there are only a few percolating paths. In particular, at the percolation threshold there is only one percolating backbone [61]. At relatively large porosities ($\phi > 0.90$), on the other hand, the flow fluctuations are in the form of swirls. These swirls are similar to the known dipole-like patterns for the net velocity field $\mathbf{u} - \bar{\mathbf{u}}$ of flow past a single particle [6]. Vector velocity maps for part of the flow field for flow through 2D random media are displayed in figure 2-5. One sees clearly the difference between the channelized flow and the swirls.

We can quantify the focusing at small ϕ in two ways. In figure 2-6a we plot the normalized fourth velocity moment (kurtosis or flatness, [22]),

$$M_4 = \frac{\langle u^4 \rangle}{\langle u^2 \rangle^2}. \tag{2.6}$$

As seen in the figure, for porosities larger than $\phi_c \simeq 0.77$, M_4 is approximately constant, as expected when P_u is Gaussian. On the other hand, for porosities less than ϕ_c, M_4 increases with decreasing porosity. Comparing with figure 2-4, we see that ϕ_c is approximately the critical porosity below which the flow is focused.

Since M_4 depends on the porosity, one expects that the form of the PDF P_u does

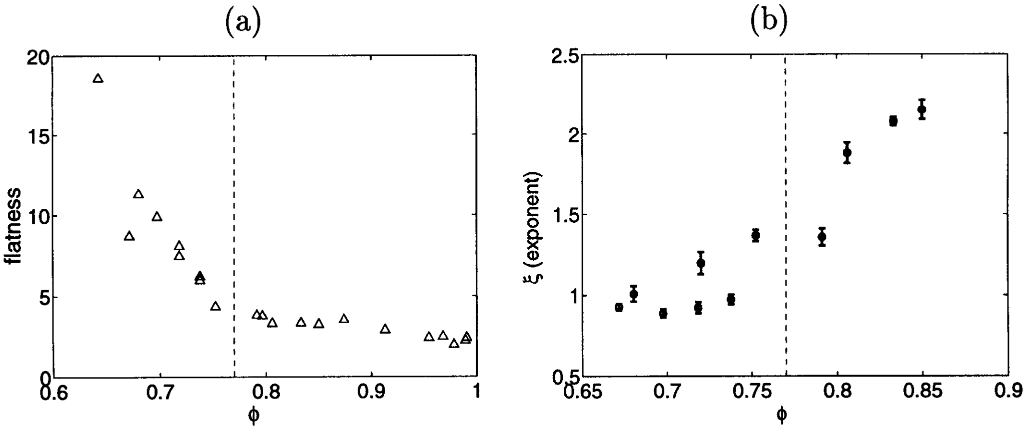

Figure 2-6: (a) Flatness versus ϕ. (b) Exponent ξ of equation (2.7) versus ϕ. The vertical dashed line in both figures intersects the abscissa at $\phi = 0.77$. In (a) one clearly observes a transition in behavior of the flatness at $\phi_c \simeq 0.77$. The transition separates channels ($\phi < \phi_c$) from swirls ($\phi > \phi_c$).

also. We find that the exponential tails of figure 2-3 are in fact a special case of the stretched exponential form

$$P_u(u/\bar{u}) \propto \exp\left[-\beta(u/\bar{u})^{\xi}\right]. \tag{2.7}$$

We have fit this form to a subset of the same data used in the measurements of M_4 and the result is shown in figure 2-6b. We find that for decreasing porosities $\phi < \phi_c$ the exponent $\xi \rightarrow 1$. Conversely, for increasing porosities $\phi > \phi_c$, $\xi \rightarrow 2$. These bounds for ξ are important and will reappear later in our theoretical discussion.

In summary, we have found that the fast part of the flow through low porosity random media is organized in channel-like patterns for $\phi < \phi_c$, whilst at large porosities, the flow exhibits swirls. The velocity PDF's are also different for different porosities. Specifically, the velocity fluctuations of the swirls are Gaussian, whereas for $\phi < \phi_c$, the velocity PDF's decay exponentially at relatively fast velocities. In the remainder of the chapter we concentrate exclusively on the low-porosity channelized flow.

2.5 Properties of channelized flow

The channels of the low porosity flows can be isolated from the relatively slow background by thresholding the velocity field. Figure 2-7 displays such a construction, where here we have chosen the threshold velocity $u_{th} = \bar{u}$, where $\bar{u}$ is the mean speed. The same figure displays three streamlines. The streamlines can be used to compute the effective thickness h of the channels to which they belong. To do so, let $p(\tau)$ denote the streamline. The local channel width $h(\tau)$ is dynamically defined by the velocity as the width

$$h(\tau) = \int_{\Omega(\tau)} d\tau_{\perp} \tag{2.8}$$

of an interval $\Omega(\tau)$, where

$$\Omega(\tau) = \left\{ \tau \,|\, u_{||}(\tau_{\perp};\tau) \geq u_{th} \right\}. \tag{2.9}$$

Here, $u_{||}$ is the component of the velocity in the direction tangent to the streamline and $\tau_{\perp}$ is the displacement in the direction perpendicular to the local tangent at position τ. The variations of the dynamic channel thickness h, the channel flux

$$\psi(\tau) = \int_{\Omega(\tau)} u_{||}(\tau_{\perp};\tau)\, d\tau_{\perp}, \tag{2.10}$$

and the channel velocity,

$$\hat{u}(\tau) = \psi(\tau)/h(\tau) \tag{2.11}$$

along an arbitrarily chosen streamline are depicted in Figure 2-7.

The three quantities $h(\tau)$, $\psi(\tau)$ and $\hat{u}(\tau)$ are each depicted in figure 2-8 for a specific channel. Their most important feature is the large peaks or bursts. These bursts are due to the branching of the channel into other channels. The quantities $h(\tau)$, $\psi(\tau)$ and $\hat{u}(\tau)$ are also clearly correlated to each other; whenever there is a sudden change in, say the channel width, there is a sudden change in both the flux and the average channel velocity too. Note that, the paths are special cuts through the medium, since one expects (and we have verified) that the velocities are more

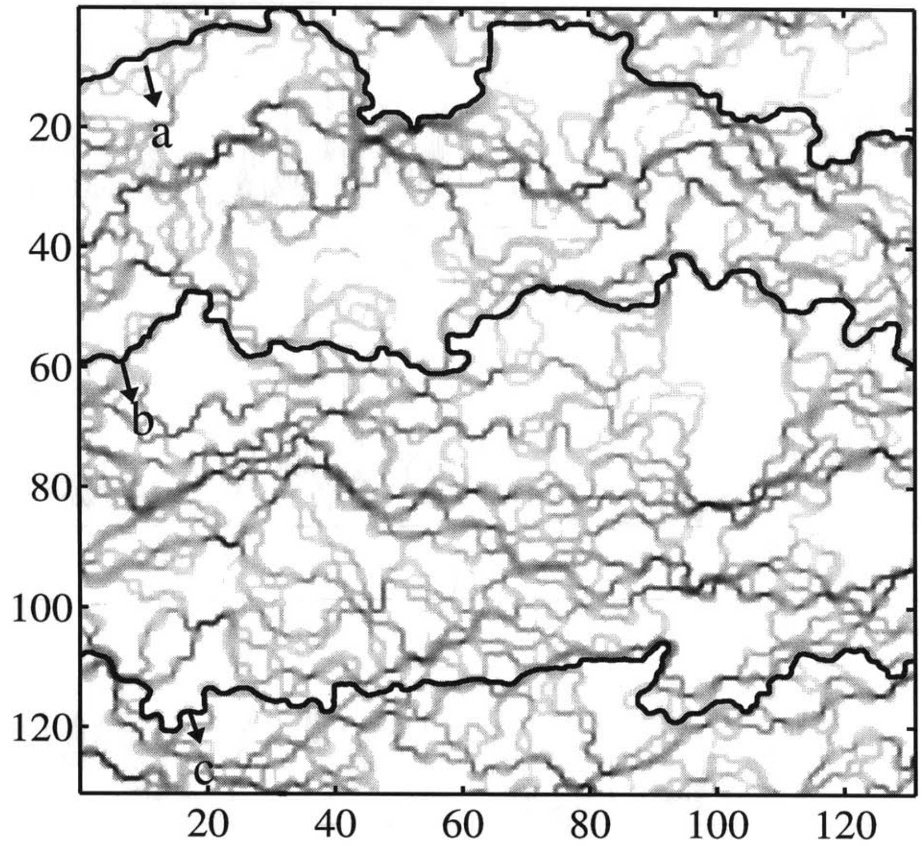

Figure 2-7: Intensity plot of the velocity $u = |\mathbf{u}|$. The flow field correspond to flow through a 2D Poisson medium on a square lattice with a porosity $\phi = 0.68$. The axis labels are in units of the grain size d and the external forcing direction is from left to right. The three streamlines a, b and c are colored black.

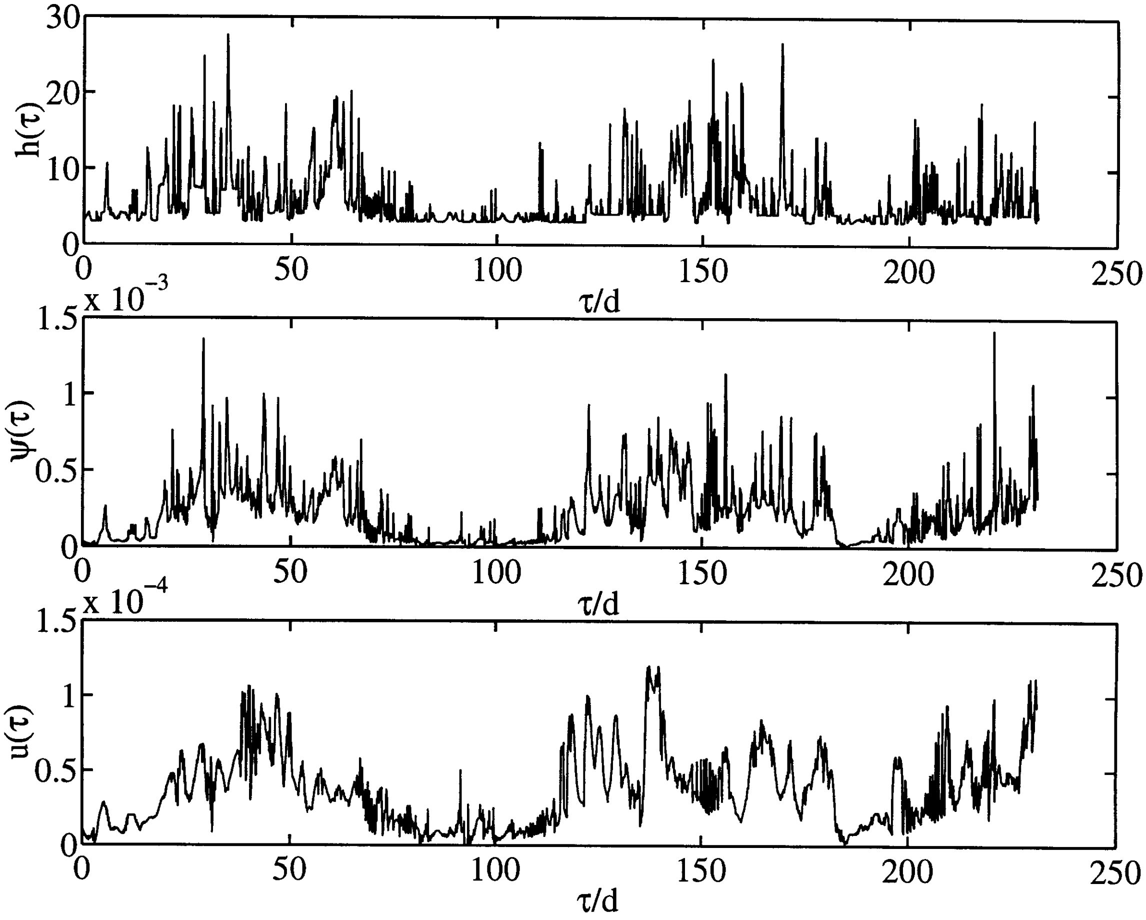

Figure 2-8: Plots of the three dynamical channel properties h, ψ and $\hat{u}$ for path a of Figure 2-7. The large peaks or bursts in all three panels of the Figure are due to branching.

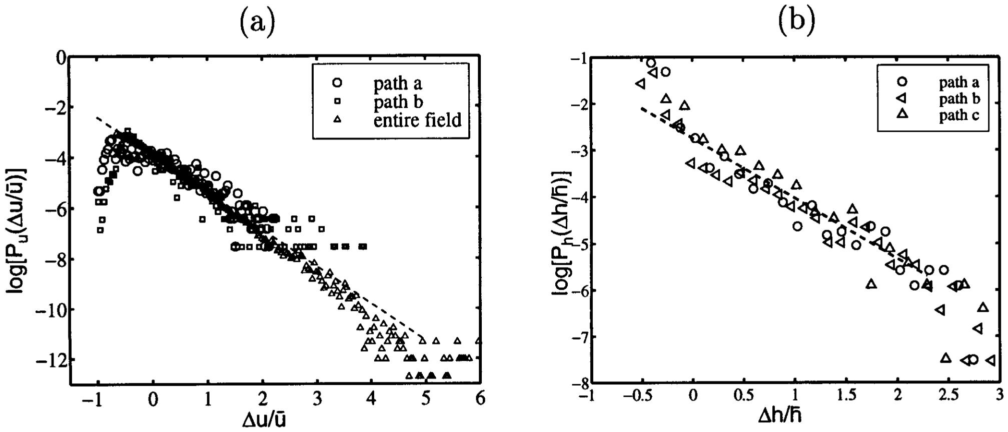

Figure 2-9: PDF's for $\hat{u}$ and h. (a) Probability distributions of the relative averaged channel velocities for paths a (circles) and b (squares) of figure 2-7 and the entire interstitial velocity field $|\mathbf{u}(\mathbf{x})|$ (triangles). Remarkably, the velocity distribution of each path decays with an equal rate. The rate of the decay in $P(\hat{u}/\bar{u})$ for the channel velocities as well all pore velocities is $\beta = 1.48 \pm .03$. (b) PDF of h. The slope is $\alpha = 1.29$.

strongly correlated along the paths than they are along any other cut through the medium. On the other hand, the decay of the PDF P_u of the velocity fluctuations is the *same* for any throughgoing path and the entire velocity field: both decay according to the stretched exponential form (2.7). This observation, which is demonstrated in figure 2-9a, is fundamental. In particular, our theoretical development in section 2.6 will exploit this correspondence to explain the stretched exponential tails in the entire velocity field.

The width $h(\tau)$ of the channel is also exponentially distributed, as can be observed in figure 2-9b. Like the distribution of the velocity fluctuations, the exponential distribution of the channel width is presumably a generic feature of flow through porous media. Explicitly, we find that

$$P_h(h(\tau)/\bar{h}) \propto \exp\left[-\alpha h(\tau)/\bar{h}\right], \qquad (2.12)$$

where $\bar{h}$ is the channel width averaged over the entire path.

The distribution of the flux ψ is qualitatively different. Since the losses and gains in the flux along the channel are on average equal, there is approximately an equal amount of channels joining as well as leaving the path. These fluctuations are instantaneous at each branching of the path. The PDF $P_{\hat{u}}(\hat{u})$ for the channel velocity depends on the fluctuations of the flux $\psi(\tau)$ and the variations of the width $h(\tau)$. This can be formally expressed by

$$P_{\hat{u}}(\hat{u}) = \int_0^\infty P_{\hat{u}|\psi}(\hat{u}|\psi) P_\psi(\psi)\, d\psi, \tag{2.13}$$

where $P_{\hat{u}|\psi}(\hat{u}|\psi)$ is the conditional PDF of the velocity given the flux and $P_\psi(\psi)$ is the PDF of the flux itself. Obviously, if the flux is conserved or branching does not exist, $P_\psi(\psi) = \delta(\psi - \psi_0)$. For more general situations, we can compute P_ψ by first computing $P_{\hat{u}|\psi}$. The latter PDF can be easily obtained from the relation $\psi = \hat{u}h$ and equation (2.12). In this way, one obtains

$$P_{\hat{u}|\psi}(\hat{u}|\psi) \propto \hat{u}^{-1} \exp\left[\frac{-\alpha\psi}{\hat{u}}\right]. \tag{2.14}$$

The PDF P_ψ can then be computed from equation (2.13) by substituting the conditional PDF (2.14) into equation (2.13) and assuming that $P_{\hat{u}}$ is known. The general solution is

$$P_\psi(\psi) \propto \mathcal{L}^{-1}\left\{\alpha/s\, P_{\hat{u}}(\alpha/s)\right\} \tag{2.15}$$

where $\mathcal{L}^{-1}$ is the inverse Laplace transform. For the case $P_{\hat{u}}(\hat{u}) = \exp(-\beta\hat{u})$, equation (2.15) gives

$$P_\psi(\psi) \propto J_0\left[2\sqrt{\alpha\beta\psi}\right], \tag{2.16}$$

where J_0 is the zero-order Bessel function. This prediction is compared against a histogram of ψ in figure 2-10. The qualitatively good fit shows that our extraction of the channel properties h, ψ and $\hat{u}$ has produced functions that are statistically consistent with each other in addition to satisfying the relation $\psi = \hat{u}h$. Moreover, the fact that $P_\psi \neq \delta(\psi - \psi_0)$ implies that the leakage of the channel cannot be ignored.

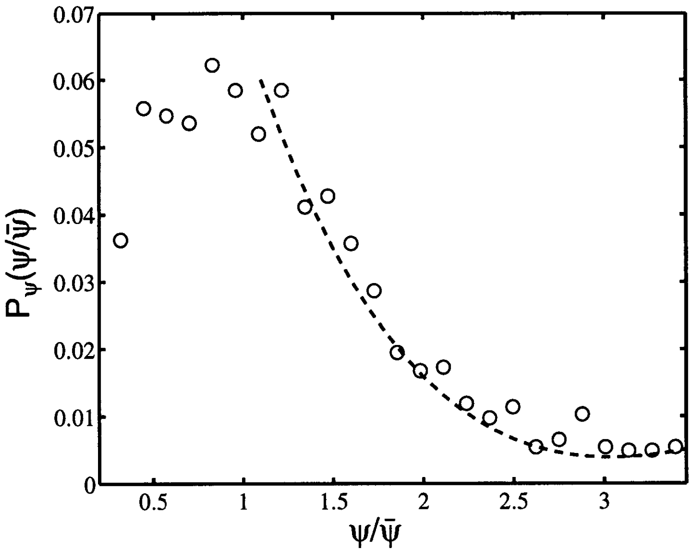

Figure 2-10: Comparison of flux distribution measured along path *a* (circles) for the flow field of Figure 2-7 with the prediction (2-10) (dashed line).

2.6 Leaky channel model

2.6.1 Failure of unconnected channels

The fundamental observation of exponential tails in the entire velocity field of low-porosity flows requires an explanation. Maier et al. [36] attempted to explain this with a simple model composed of unconnected isolated pipes with stochastically varying diameters. In our notation, their model assumes that $\hat{u} \propto h^2$, so that

$$P_{\hat{u}}(\hat{u}) \propto P_h(\sqrt{h}) \left| \frac{d\,h}{d\,\hat{u}} \right| . \tag{2.17}$$

This model, however, is inconsistent with our observations. Given the exponentially decaying form (2.5) for P_h, one obtains

$$P_{\hat{u}} \propto \hat{u}^{-1/2} \exp\left[-\beta\sqrt{\hat{u}}\right] \tag{2.18}$$

from (2.18). We found, however, in section 2.4 that the exponent ξ is always larger than 1, whereas equation (2.18) implies $\xi = 1/2$. This failure is due to a fundamental problem: the pipes are unconnected. Thus in the following section we introduce a

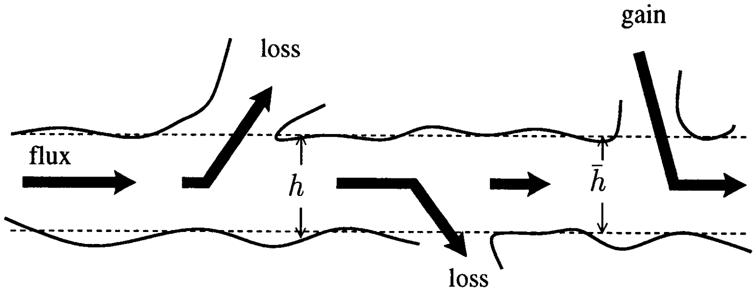

Figure 2-11: The leaky single channel model. In this model both the width h and the flux vary along the channel. The flux varies due to branching. The nominal channel walls are indicated with straight dashed lines and separated by the amount $\bar{h}$.

model in which the connectivity of the channels plays an integral role.

2.6.2 Stochastic channel equation

Our explanation of the exponential tails in the PDF P_u of the entire velocity field begins with the observation in section 2.5 that the PDF $P_{\hat{u}}$ of the channel velocity is also exponential. Since the flow through low porosity media is strongly focussed into channels, and the fastest velocities occur in these channels, we conclude that the tails of P_u derive directly from $P_{\hat{u}}$. Thus we concentration our attention on the channel-velocity PDF $P_{\hat{u}}$.

Central to our approach is that each of our channels is leaky. Specifically, as we have already pointed out, the channel flux ψ is not constant; indeed it is highly fluctuating, as a consequence of leakage in and out of the channel due to branching. A cartoon of this model is depicted in figure 2-11.

In our leaky channel model, fluctuations of $\hat{u}(\tau)$ result not only from branching but also from variations of the effective channel width h. Taking $\kappa \propto h^2$ to be an effective permeability representing the branching by a fluctuating random process f, we model the fluctuations of $\hat{u}$ by the Langevin equation

$$\frac{d\hat{u}(\tau)}{d\tau} = -\left[\kappa(\tau)\right]^{-1} \hat{u}(\tau) + f(\tau). \tag{2.19}$$

Here τ, as before, denotes the distance along path.

For the case of a plane channel with solid walls, equation (2.19) reduces to the classical channel equation $\hat{u} = \kappa f$, where f is a constant pressure gradient. In the leaky channel model both κ and f are fluctuating quantities. The fluctuations in the forcing f are due to the fluctuations in the flux (i.e., branching) and the fluctuations in κ are due to the fluctuations in the channel width. We emphasize once again that the fluctuations of f imply that the flux across the channel is not conserved.

In principle, when the fluctuations in κ and the fluctuations in f are specified then the velocity distribution for P_u can be obtained. Many statistical properties of the fluctuations f can be derived indirectly from the discussion of the channel quantities h and ψ in previous sections. Practically, however, it turns out to be very difficult to obtain velocity PDF's for stochastic equations like equation (2.19). Because of the latter difficulties we necessarily have to simplify the statistical behavior of the noise terms κ and f.

First, we assume that $f(\tau)$ is normally distributed, which is in reasonable agreement with the empirical PDF of ψ plotted in figure 2-10. We also assume that the f and κ are uncorrelated, such that

$$\langle k(\tau) f(\tau') \rangle = 0, \qquad (2.20)$$

and that the autocorrelations satisfy

$$\langle f(\tau) f(\tau') \rangle = \delta(\tau - \tau'), \qquad (2.21)$$

$$\langle \kappa(\tau) \kappa(\tau') \rangle = \delta(\tau - \tau'). \qquad (2.22)$$

Visual inspection of figure 2-8, however, shows some correlations between h and ψ. Moreover, we have already indicated that $\hat{u}$ is relatively correlated along the path. Nevertheless, we may hope that, as is common in statistical mechanics, an uncorrelated "mean field" theory can produce useful results.

In the appendix, we show that these assumptions allow us to derive [19] the stretched exponential form (2.7) from the stationary solutions of the stochastic channel equation (2.19). Importantly, the phenomenological stochastic channel equation predicts that the exponent ξ in (2.7) is bounded such that $1 \leq \xi \leq 2$, which is in good agreement with our observations.

2.7 Conclusions

Our simulations of flow through random porous media show that the velocity fluctuations in low porosity media are organized into localized, channel-like patterns, whereas the velocity fluctuations in high porosity media are in the form of swirls. The transition between the two patterns is well defined in terms of the statistical moments of the velocity fluctuations. Specifically, the swirls correspond to Gaussian distributed velocity fluctuations and the channel-like patterns correspond to velocity PDF's with exponential tails. For our particular random 2D porous media, this transition occurs at a porosity $\phi_c = 0.77$. The sharpness of this transition is surprising, and remains unexplained.

We have performed a detailed study of the low porosity channelized flows. We have shown that the low porosity flow is organized in strongly branching channel networks and that the velocity field of the flow is exponentially distributed. We then constructed a simple, phenomenological model for the fast part of the flow in random porous media. The aim of this model is similar to Brinkman's [12] model for suspensions: Specifically, we seek an interim model at a slightly large scale than the pore scale but at a smaller scale than the one set by Darcy flow. In our model the flow through the entire porous media is represented by a single channel with leaky, slowly modulating channel walls. Channels are defined as the fast part of the flow along an arbitrary streamline.

We have cast the channel model in the form a stochastic differential equation. In this equation, the flow is the response to (1) a damping force due to variations in the channel width, and (2) a separate forcing due to flux variations. Under the assumption that both forcing terms are uncorrelated, this stochastic equation yields exponential velocity distributions. This result is in good agreement with the observations that the channel velocity also decays exponentially. We emphasize that our leaky channel model is fundamentally different than all other channel models for flow through porous media [53, 36], because it integrates the connectivity of the channel through fluctuations in the channel flux.

It would be desirable to extend our work to obtain better estimates of bulk transport properties. To estimate the permeability we, note that, once the typical length scale $l = \alpha^{-1}$ of the channel is known and the number of channels per unit area is known, a prediction of the permeability k could be $k \propto nl^2/12$ in two dimensions. Such an expression, however, must be supplemented by an additional factor that represents an effective slip due to leakage [9, 51].

An important extension of our work lies in the field of hydrodynamic dispersion [50, 29]. Obviously, the leakage of our channel is an essential feature of the dispersion of a passive scalar field. Precisely how to make this connection, however, remains a subject for future research.

Chapter 3

Patterns in slow flow through dilute fixed particle clouds

Abstract

We study the statistical properties of slow flow through dilute, non mono-dispersed, fixed particle clouds. Numerical simulations show that the flow in this high porosity limit exhibits swirls. We find that both the velocity fluctuations and the characteristic swirl size have a power-law dependency on the solid volume fraction. By means of a scaling argument, we show that the correlation length of the swirls scales like the mean distance between particles. We find that, for relatively large values of the solid fraction, the swirls disappear and that channel-like patterns can be observed instead. Inspection of the behavior of the velocity fluctuations indicates that there is a sharp transition from swirls to a predominantly channelized flow.

3.1 Introduction

Recent experiments by Segré et al. [57] demonstrate that the fluctuations in the macroscopic settling velocity of particles exhibit large-scale finite-range correlations in the form of swirls. They find that these swirls have an amplitude and a characteristic swirl size that depend in a remarkably simple way on the solid fraction η. Their main results are that the velocity fluctuations are of order $\eta^{-1/3}$ and that the swirl size is of order $\eta^{1/3}$.

Motivated by these observations, we examine velocity fluctuations in slow flow through two dimensional fixed arrays of particles. The purpose of this present paper is to verify whether the observed simplicity in the (particle) flow phenomenology of sedimenting suspensions can also be observed in fixed particle clouds. Since both the sedimenting structures and fixed particle clouds may be interpreted as porous media [12], any insight into either one could yield insight into the other.

To achieve this goal, we use two dimensional numerical simulations of Stokes flow through two dimensional porous media to obtain the velocity field. The properties of the random media model used in this study depend on the solid fraction η. In particular, the porous model is a mono-dispersed fixed particle array for $\eta < 0.02$ and become multi-dispersed for larger η due to clustering of the particles.

We find that for low solid fractions ($\eta < 0.2$), the velocity fluctuations in the fluid flow behave in a qualitatively similar way as Segré's results for suspensions. Specifically, the velocity fluctuations manifest themselves as swirls. Their amplitudes saturate at $U_z \eta^{0.21}$, where U_z is the average velocity in the applied forcing direction and their correlation length is of order $\eta^{-0.41}$, where d is the grain size. Remarkably, we find that the latter scaling behavior for the swirls extends to values of η for which the porous media is actually multi-dispersed as opposed to mono-dispersed.

These scaling behaviors are not entirely new [12, 18, 35, 27], insofar as mono-dispersed particle arrays are concerned. To the best of our knowledge they are new, however, for multi-dispersed media. Interestingly, we shall show that the scaling behavior of the typical swirl size can be explained with a model due to Brinkman [12], which has been derived for dilute mono-dispersed particle clouds. By means of a scaling argument, we show that the the correlation length of the flow depends on η in nearly the same way as the average particle distance does.

For large η, we find that the swirls vanish giving way to more focussed, channelized patterns. Computations of the velocity fluctuations indicate that the transition to the channel-like flow pattern is rather sudden. At this transition, the velocity fluctuations are of an order equal to the averaged velocity.

This paper is structured as follows. First, we briefly discuss our model porous structure and the numerical method employed. We next discuss our results for dilute media and provide some theoretical explanations. Finally, we discuss the detrimental effects of large solid fractions on the swirls.

3.2 Fluctuations of flow in dilute particle clouds

3.2.1 Numerical method and porous medium model

To simulate Stokes flow we employed the Lattice Boltzmann method [46], which is particularly well suited to the simulation of flow through complex structures. Periodic boundary conditions are imposed in all simulations.

The media were constructed on a square lattice of size $L \times L$ lattice sites. To each site of the lattice a random number was assigned. Whenever,the random number at a lattice site is larger than a given threshold probability $1 - \eta$, the site was identified as a particle or solid site. To obtain square shaped particles of size d, the above construction has been performed on a coarse grained lattice with dimensions $L/d \times L/d$. For small values of η this porous model yields mono-dispersed media. However, for $\eta \geq 0.02$, a significant number of grains stick together to form larger grains. In this case, the medium can no longer be regarded as mono-disperse.

3.2.2 Results from simulations

Velocity fields have been obtained for simulations of Stokes flow through the above random 2D structures. We find that, for relatively small solid fractions the velocity fluctuations take the form of swirls. Figure 3-1 displays part of the vector field of the flow taken at two small solid fractions, $\eta = 0.0056$ and $\eta = 0.041$. For this figure the simulations are performed on a lattice with size 256×256 and with square grain size $d = 4$. As can be clearly observed in the figure, the swirls become more apparent at smaller values of η.

To obtain estimates for the swirl size, we have studied the velocity-velocity correlation functions. The correlations of velocity component u_i in direction x_j can be

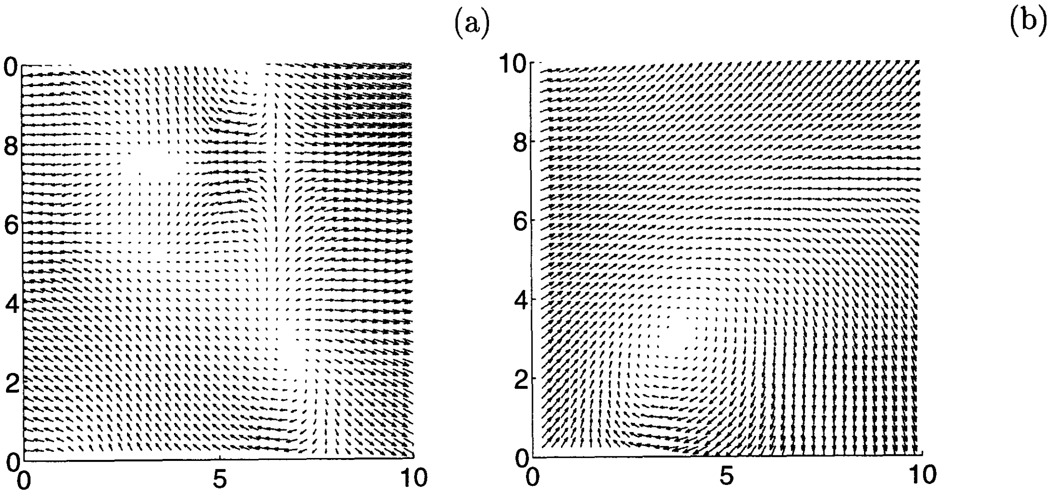

Figure 3-1: Vector velocity maps for part of the flow fields $\mathbf{u}-\bar{\mathbf{u}}$, where $\bar{\mathbf{u}}$ is the mean velocity. (a) $\eta = 0.041$. (b) $\eta = 0.0056$. The main flow direction is from left to right. Note that the swirls in (a) are smaller than in (b).

defined as

$$C_i(x_j) = \frac{\langle \tilde{u}_i(x_j)\tilde{u}_i(0)\rangle}{(\Delta U)^2} \tag{3.1}$$

where $\tilde{u}_i(x_j) = u_i(x_j) - \langle u_i \rangle$, where $\langle u_i \rangle$ denotes the average velocity. The insets in figure 3-2 show two of these correlation functions: $C_z(x)$, the correlations of the horizontal velocity in the vertical (forcing) direction, and $C_z(z)$, the correlations of the vertical velocity in the vertical direction. Both cases are plotted for four different solid fractions η. The larger plots in Figure 3-2 show these same correlation functions, after rescaling of the lag x_j by $\eta^{-0.42}$. Quite noticeable are the collapse of the correlation functions in both lag directions for small lag (before finite-size effects degrade the data).

For a series of simulations of flow through fixed particle clouds with low solid fractions η, we have computed the averaged amplitude of the velocity fluctuations in the forcing direction, estimated by

$$\Delta U = \langle [u - \langle u \rangle]^2 \rangle^{1/2}. \tag{3.2}$$

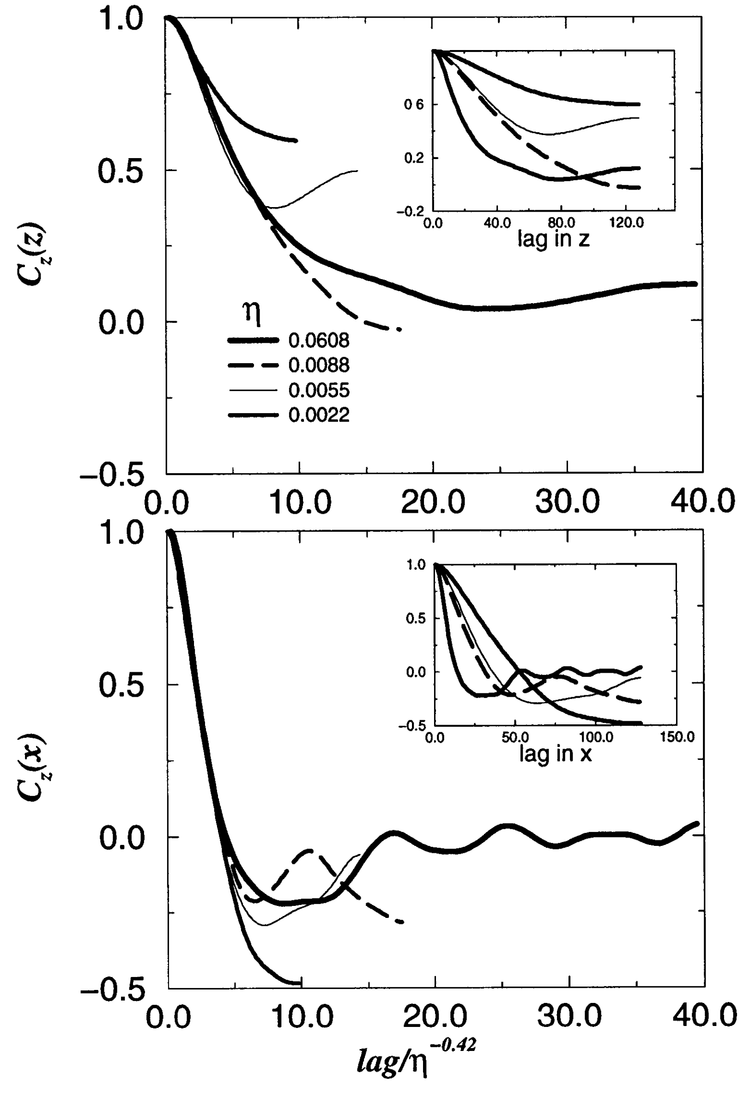

Figure 3-2: Spatial correlation functions of the velocity component in the forcing direction as a function of the lag, for different values of the solid fraction η. The lag z in the top figure is in the direction of the forcing, while the lag x in the bottom figure is perpendicular to the forcing direction. The lags in the insets are unscaled, while the lags in the large figures are rescaled by $\eta^{-0.42}$.

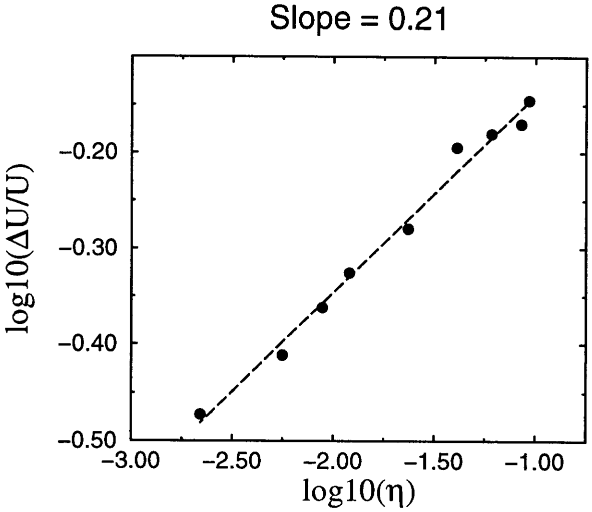

Figure 3-3: Normalized velocity fluctuation amplitudes $\Delta U/U$ versus solid fraction η.

Figure 3-3 shows that the data can be well fitted by

$$\frac{\Delta U}{U} \sim \eta^{0.21} \simeq \eta^{1/5}, \tag{3.3}$$

where $U = \langle u \rangle$. Remarkably, since η is large, the scaling relation (3.3) appears to be also valid for multi-dispersed media. This fact is even better illustrated in figure 3-6.

In summary, we thus find that the velocity fluctuations in dilute, multi-dispersed fixed particle "clouds" behave nearly the same way as the flow associated with the settling of suspensions. We find that the typical swirl size scales like $\eta^{0.21}$ and that the velocity fluctuations saturate at $\eta^{-0.42}$.

3.2.3 Theory

In this section, we begin with a prediction of the scaling behavior of the correlation length or typical swirl size. Using scaling arguments, we then show that the correlation scales in a similar way as the average particle distance.

A simple model for slow flow in dilute and random mono-disperse random media is the one of Brinkman's [12]. This model is noteworthy, since previous studies [18, 35, 51, 27] have theoretically justified Brinkman's model for low solid fraction η. The empirical Brinkman's equation [12] describes slow flow of a particle embedded in a dilute porous medium with particle density n. Brinkman's equation can be written as

$$
\begin{aligned}
-\nabla p + \tilde{\mu}\nabla^2\mathbf{u} - \tilde{\mu}\alpha^2\mathbf{u} &= 0 && (3.4)\\
\nabla\cdot\mathbf{u} &= 0, && (3.5)
\end{aligned}
$$

where α^{-1} is a typical length scale and $\tilde{\mu}$ is an effective viscosity [12, 35] of the dilute medium. Brinkman's equation is Stokes equation plus an additive Darcy or damping term $\tilde{\mu}\alpha^2\mathbf{u}$, to incorporate the effects of the porous mass. For distances beyond α^{-1} the flow does not experience the contribution of a single individual particle. Thus, α^{-1} corresponds to the characteristic size of the swirls. In Brinkman's original model, this length scale is proportional to $\sqrt{k}$, where k is the permeability of the random fixed particle cloud. In this case, the term $\tilde{\mu}\alpha^2$ corresponds to the total drag coefficient of the fixed suspension.

Since equation (3.4) applies to spherical particles, we will assume that the square-shaped grains in our porous model can be regarded as spherical grains with diameter d. The latter assumption is reasonable when $\alpha^{-1} \gg d$, which is the case for small η. The boundary conditions for Brinkman equations are

$$
\begin{aligned}
\mathbf{u}(\mathbf{x}) &= 0 \text{ for } |\mathbf{x}| = d/2 && (3.6)\\
\mathbf{u}(\mathbf{x}) &\to \mathbf{U} \text{ for } |\mathbf{x}| \to \infty, && (3.7)
\end{aligned}
$$

where $\mathbf{U}$ is the average velocity of the flow.

Let $\mathbf{F}_D$ denote the drag on a single particle, as calculated by solving Brinkman equations subjected to the boundary conditions (3.6), (3.7). Then, the total drag on the dilute system equals $\tilde{\mu}\alpha^2\mathbf{U}$ or

$$
n\underline{\mathrm{F}}_D = \tilde{\mu}\alpha^2\mathbf{U}. \qquad (3.8)
$$

The latter relation results in equation for α. In two dimensions, the drag [27, 52] on

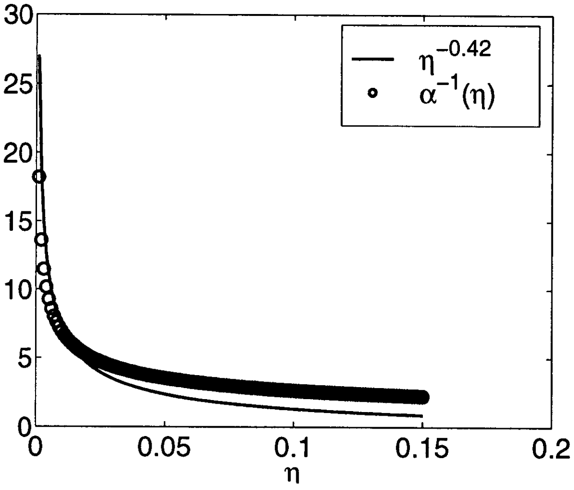

Figure 3-4: Brinkman's result (solid line) for the characteristic swirl size l_s (circles) versus η obtained from data collapse of the autocorrelation function in figure 3-2.

a single particle is given by

$$\mathbf{F}_D = 4\pi\mu\left[\alpha d K_1(\alpha d)/K_0(\alpha d) + \frac{1}{2}\alpha^2 d^2\right]\mathbf{U}, \tag{3.9}$$

where K_i is the modified Bessel function of integer order i. Since we are interested in the dependence of the normalized length on η, we may choose $r = d/2 = 1$. Substitution of equation (3.9) into the drag balance, equation (3.8) yields the following equation for α,

$$\alpha = \frac{2\alpha K_1(\alpha)}{K_0(\alpha)(\frac{1}{2}\eta - 1)} \tag{3.10}$$

We have numerically solved (3.10) for α for various values of η. The result is plotted in Figure 3-4. From the latter figure it is clear that the functional dependence of α^{-1} is very similar to the numerically obtained relation.

Interestingly, the following scaling argument for the average particle separation gives a functional dependence on η, which is surprisingly similar to the characteristic swirl size l_s. Let N be the number of particles in a box of size $L \times L$. Ignoring the particle size, the average distance l_p between the particles is $l_p \approx \sqrt{L^2/N} = L/\sqrt{N}$. Let d denote the grain diameter. The solid fraction is $\eta = Nd^2/L^2 \propto N/L^2$. Hence, the particle distance scales like

$$l_p \propto \eta^{-0.5}. \tag{3.11}$$

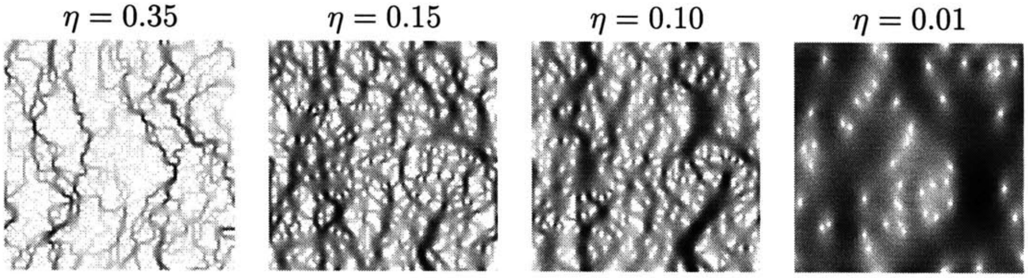

Figure 3-5: Intensity plots of $|\mathbf{u} - \bar{\mathbf{u}}|$ for different values of η. The fastest velocities are colored in black. Note that, the channels are completely vanished at $\eta = 0.01$.

Despite the simplicity of the argument, the match between average spacing of the particles $l_p \propto \eta^{-0.5}$ and the the typical swirl size $l_s \propto \eta^{-0.42}$ is at the very least surprising.

The drag of one single particle is needed, in order to predict the behavior of the relative velocity amplitude. It is well known that for 2D Stokes flow, the leading behavior of the velocity is proportional to $\log(|\mathbf{x}|)$. Thus the velocity field is singular at large distances and therefore, the drag on a single particle is not defined. The singularity can be removed by using the Oseen approximation [6]. Such an approach would, however, dramatically increase the difficulty of the problem. A prediction for the velocity amplitudes is in progress.

3.3 The vanishing of swirls

For large η, the swirls vanish and channel-like patterns can be observed instead. Figure 3-5 displays this transition. Moreover, the scaling for the velocity fluctuation does not hold for all values of η, as demonstrated in figure 3-6. There appears to be a well defined range for power-law behavior of the velocity fluctuation. Specifically, for our porous medium model, the scaling for the velocity fluctuations (3.3) holds for $\eta < \eta_c = 0.23$. Of note also is that, the velocity fluctuations are about equal to zero for $\eta \simeq \eta_c$.

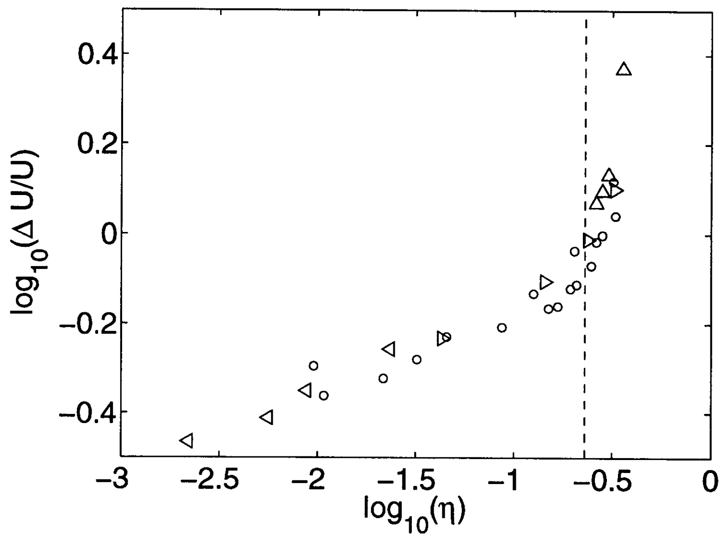

Figure 3-6: Normalized velocity fluctuation amplitudes $\Delta U/U$ versus and solid fraction η. The vertical dashed line intersects the abscissa at $\eta = 0.23$. One clearly observes a transition in the amplitude $\Delta U/U$ at $\eta \simeq 0.23$. The transition separates swirls $\eta < \eta_c$ from channels $\eta > \eta_c$.

3.4 Conclusions

New observations of slow flow in particle clouds are presented. We show that the velocity fluctuation in flow through dilute fixed particle arrays behave in similar way as the velocity fluctuations of the particles in sedimenting suspensions. It is found that Brinkman's model provides a reasonable estimate for the characteristic size of the swirls. Moreover, it has been shown that this size can be estimated from the average distance between the particles. These swirls are not found in tight porous media; where, rather channel-like patterns can be observed. Inspection of the behavior of the velocity fluctuations indicates that there is a sharp transition from swirls to a predominantly channelized flow.

Chapter 4

Critical behavior in flow through a rough walled channel

Abstract

We study flow through a single fracture by numerical simulation and present a theory for single fractures and networks of tight fractures that predicts scale dependency of the transport properties. The fracture is modeled as a rough channel bounded by two self-affine fractal surfaces. Flow fields are obtained from numerical simulations using 3D lattice gas methods which solve the Navier-Stokes equations. The flow simulations are performed at low Reynolds number. It is in this regime that we study the effect of the surface topography on the flow for various values of the mean aperture of the fracture. For the case of tight uncorrelated channel walls we predict a power law dependency of the permeability on the length of a single fracture measured in the direction of the main pressure gradient.

4.1 Introduction

For many geological structures fractures are the dominant conduit for fluid transport [66]. An example is a sedimentary basin, where the flow can be predominantly in a particular fault or through a network of faults. Most often the fractures are almost closed. Thus, the study of flow through tight fractures is a key component in the understanding of transport phenomena in geological structures and fracture networks.

Fractures in a rock are commonly described by a parallel plate model. For this model the steady state solution of the Navier Stokes equations yields the so-called "cubic law" [66], where the flow rate Q across the model is proportional to the applied pressure gradient ∇p and the cube of the channel height d:

$$\mathbf{Q} = -\frac{d^3}{12\mu}\nabla p.$$

Here μ is the dynamic viscosity.

The plane channel is an oversimplified model for a real fracture, since such a model does not account for the tortuosity of the streamlines and the effect of contact regions between the fracture walls. In the past, the description of flow through a rough-walled channel has been thought to entail lubrication theory [13]. In the lubrication approximation [6], or, equivalently in the low Reynolds number regime and for slowly varying and slightly rough fracture walls, the Navier-Stokes equations can be approximated by the so-called two-dimensional Reynolds equation [41]. However, at relatively small channel widths, the amplitudes of the dominant wavelengths of the rough channel are too large for the Reynolds approximation to hold [38]. Thus in our simulations we solve the three dimensional Stokes equations and measure the transport properties of the flow.

Of great interest is the point of transition where the fracture becomes closed, and stops conducting the flow. Here, we shall show that this point is a critical point that corresponds to a phase transition. Consequently, the transport properties of the flow through tight fractures are scale dependent. An important extension of this theory is to flow through fracture networks. We conclude this paper with a theory for the permeability of a simple fracture system.

4.2 Simulations

Fracture model: A single fracture can be described by the void space between two rough surfaces. The mean separation between the two surfaces is called the mean aperture. Statistics obtained for the surfaces of a fracture show that many fracture surfaces are self-affine (i.e., fractal) [55] . A characteristic statistical parameter of a self-affine surface is the roughness exponent ζ, which is related to the fractal dimension D by $D = 3 - \zeta$ [64, 62]. Measurements of fracture surfaces for numerous brittle and ductile materials typically give a roughness exponent of about 0.85 [47, 55]. To simplify our model we assume that the fracture surfaces are isotropic. The assumption of isotropy seems reasonable, since isotropy has been observed in certain rock types such as granite [55]. Here, Gaussian fractal surfaces are constructed by the Fourier filtering method [62] and have the additional property that they are periodic in all directions. Fractures are then formed by juxtaposing two independent realizations of self-affine isotropic fractal surfaces with the same roughness exponent, $\zeta = 0.85$. While it is known that the fractures often are correlated [13], we have chosen to study the case of uncorrelated surfaces. The lack of correlation between or "matedness" of the fracture walls certainly limits the applicability of this study. However, even for relative small displacements along the fracture, the surfaces are effectively becoming uncorrelated. Thus our assumption of uncorrelated surfaces is still reasonable for a large class of fractures. Thus our fracture surfaces with roughness $\zeta = 0.85$ have a fractal dimension of 2.15. We denote $h_1(x, y)$ for the position of a fracture surface relative to a horizontal reference plane and $h_2(x, y)$ for the position of the second fracture surface. Then, as shown in figure 4-1, the aperture surface $d(x, y)$ is defined to be the distance between the two fractal surfaces [14], i.e., $d(x, y) = h_2(x, y) - h_1(x, y)$. Note that the aperture $d(x, y)$ can become negative with this definition. In our model, however, the deformation associated with surfaces in contact is ignored, and the surfaces dissolve to become part of the surrounding solid. We note that measurements on real fractures show that the contact areas of the deformed fracture are slightly larger than the contact area of our dissolving model [15, 47].

Methodology: To simulate Stokes flow we have employed a three dimensional lattice gas model [44, 46]. Other methods based on finite difference schemes [13, 38] have been used, but the advantages of lattice gas methods are that rough boundaries can easily be implemented and that the full set of the Navier-Stokes equations is solved.

Flow measurements: Numerical simulation of flow through fractures for various average fracture widths $\langle d \rangle$ have been conducted. Typically, the flow was simulated on a lattice of 64x64x64 nodes. For tight fractures, however, we increase the dimension perpendicular to the fracture plane in order to make sure that the flow is well resolved in the smaller openings.

For each flow simulation we computed the total volumetric flux Q in the forcing direction,

$$Q = \frac{1}{L} \sum_{\mathbf{r} \epsilon V} u(\mathbf{r}),$$

where $u(r)$ is the component of the local velocity in the forcing direction, L is the length of the fracture (figure 4-1) and V is the void space. The flow rate Q is related to the external pressure gradient or volume force g by Darcy's law,

$$Q/A = -\frac{k}{\nu} g,$$

where $\nu = \mu/\rho$ is the kinematic viscosity, k is the permeability and A is the surface area perpendicular to the flow Q. In order to compare the permeabilities of each simulation, we normalize the permeability by the permeability of a plane channel with height $\langle d \rangle$ and we scale the mean aperture $\langle d \rangle$ by the root mean square (r.m.s.) of the standard deviations

$$s_h = \frac{1}{\sqrt{2}} \sqrt{\sigma_1^2 + \sigma_2^2}, \tag{4.1}$$

where

$$\sigma_i = \sqrt{\langle h_i^2 \rangle - \langle h_i \rangle^2} \tag{4.2}$$

is the roughness amplitude of each fracture wall h_i, $i = 1,\ 2$. Over a range of different mean fracture separations we determine the permeability. Figure 4-2 shows the measured permeabilities of fractures with the varying mean widths. This figure shows that the permeability of a plane channel with height $\langle d \rangle$ overestimates the permeability of the fracture. This property has been observed by Brown [14] and more recently by Mourzenko et.al.[38]. Figure 4-2 also indicates three different ranges of the permeability. The ranges in this figure belong to tight, open, and wide open fractures respectively.

Figure 4-3 is an enlargement of figure 4-2 and shows the permeability data set of range I of figure 4-2 for tight fractures. The dashed line in this figure extrapolates the data towards the interception point d_c with the abscissa, which is the critical point below which the fractures become impermeable. While different curves, $k \to k(\langle d \rangle)$ will fit the data in figure 4-3 it is clear that the point of intercept of the extrapolating curve with the abscissa occurs at a mean aperture $\langle d \rangle \approx \frac{3}{2} s_h$. Therefore, we have found empirically that

$$d_c \approx \frac{3}{2}\sqrt{\sigma_1^2 + \sigma_2^2}. \tag{4.3}$$

4.3 Theory

We discuss a theory that predicts the critical aperture d_c. First, however, we show that the critical mean aperture $\langle d \rangle = d_c$ corresponds to the percolation threshold of a fractal surface $d(x, y)$.

Consider the aperture surface $d(x,y) = h_1(x,y) - h_2(x,y)$ and let S denote the contact area between the two surfaces, $S = \{x, y | h_1(x,y) - h_2(x,y) \le 0\}$. For open fractures S is an empty set, but for tight fractures S will not be empty and will most of the time be the union of the closed contact areas. We then define a reference aperture surface $R(x, y)$ to be the aperture $d(x, y)$ of the fracture when the two fracture surfaces first meet. The reference surface R has the property that it is fractal and that it has the same fractal dimension $D = 3 - \zeta$ as each of the fracture surfaces [28]. The contact areas in S for the case of R are degenerated to a collection of points. Let us view the process of closing the fracture from the perspective of the reference aperture surface.

From the cartoons in figure 4-4, we observe that in the process of closing the fracture, the parts of the reference aperture surface which stick below a horizontal surface are removed. The height of this horizontal cutting surface is zero when the aperture coincides with the reference aperture and increases for tighter fractures. The shaved parts of the reference fracture surface form barrier islands which impede the flow (see figure 4-4). These islands grow whenever the fracture becomes tighter and ultimately become so large that they obstruct the flow all together. In the latter case we have arrived at the percolation threshold of the reference surface. Thus the percolation threshold of the reference surface is at $\langle d\rangle = d_c$. Schmittbuhl et.al. [54] show that the percolation threshold of a fractal surface occurs at a distance

$$d_c \approx \frac{1}{2}\left(\max(R) + \min(R)\right). \tag{4.4}$$

The standard deviation $\sigma_R \approx \sqrt{\langle R^2\rangle - \langle R\rangle^2}$ is a robust estimate for the difference on the right-hand side:

$$d_c \approx \sigma_R. \tag{4.5}$$

In our fracture model, both surfaces h_1 and h_2 are independent and hence,

$$\sigma_R^2 = \sigma_{h_1}^2 + \sigma_{h_2}^2. \tag{4.6}$$

Moreover, since the variance of fractal surfaces has on average a power-law dependence on the fracture size L with exponent ζ and since both Gaussian fractal surfaces have equal roughness, their variances are approximately equal and thus

$$\sigma_R^2 \approx 2s_h^2. \tag{4.7}$$

Since the surfaces h_1, h_2 are fractal, the roughness amplitude s_h has a power law dependence on the system size L, such that $s_h \propto L^\zeta$. From equations (4.5), (4.7) and the power-law for s_h it follows that

$$d_c \approx \sqrt{2}\, s_h \propto L^{\zeta} = L^{3-D}. \tag{4.8}$$

Taylor series expansion of the permeability function $k(\langle d \rangle)$ about the critical point d_c yields the monomial

$$k(\langle d \rangle) = \frac{f^{(m)}(d_c)}{m!}(\langle d \rangle - d_c)^{m+\nu} + \mathcal{O}\left(|\langle d \rangle - d_c|^{m+\nu+1}\right), \tag{4.9}$$

where m is the smallest positive integer for which the (m)-th order derivative of the analytical part f of k evaluated at the threshold $\langle d \rangle = d_c$ is nonzero and $(d - d_c)^{\nu}$ is the non-analytical part of k. Thus close to the critical aperture d_c the permeability k behaves like a power law. In other words, since the transition of the fracture to a state of conductance is a second order phase transition, a finite size scaling relation [60] should apply,

$$k \propto \begin{cases} \xi^{-\alpha} & L \gg \xi \\ L^{-\alpha} & L \ll \xi, \end{cases} \tag{4.10}$$

where ξ is the correlation length of the mass of the barrier islands and α is some exponent. For resistor networks the conductivity has power-law dependency on the network size with a negative exponent [61]. Motivated by the assumption that there exists some (weak) relation with resistor networks, we assume $\alpha > 0$. Here, it is important to note that the area of the barrier islands, S, are not fractal [28] and thus percolation theory [61] cannot be used to obtain values for the exponents such as α.

An important application of this theory is to the prediction of the scale dependence of the permeability for networks of tight fractures. As an example, consider a bundle of disconnected tight and parallel fractures in a cube-shaped aquifer with side-length $\mathcal{D}$. As before, let the length ℓ of the fracture be measured in the direction of the flow. From equation (4.10) one expects that the overall, average permeability does not depend on a length scale for fracture with lengths $\ell \gg \xi$. On the other hand, equation (4.10) predicts that the permeability is scale dependent for fractures with lengths shorter than an upper bound, $\ell_{\max} < \xi$. Let $p(\ell)$ denote the probability density distribution of the fracture length. Then the average permeability due to the shorter, scale dependent tight fractures is

$$\langle k \rangle \propto \int_{\mathcal{D}}^{\ell_{\max}} \ell^{-\alpha}\, p(\ell)\, d\ell. \tag{4.11}$$

In particular, when $p(\ell)$ is a log normal distribution [62] the average permeability of equation (4.11) scales like

$$\langle k \rangle \propto \operatorname{erf}[-a \ln(b\, \ell_{\max}) + c\alpha], \tag{4.12}$$

where erf is the error function and a, b and c are positive constants that depend on the two free parameters of the log normal distribution. Importantly, the scaling relationships such as equation (4.12) can be tested against measurements of the permeability for different sample lengths.

4.4 Conclusions

As previous studies have shown [13, 38] a simple plane channel model is an inadequate model for a rough-walled fracture. We have developed a theory for tight fractures. In particular, the theory for our fracture model of juxtaposed and uncorrelated fractal surfaces predicts a power-law behavior of the permeability with the fracture length.

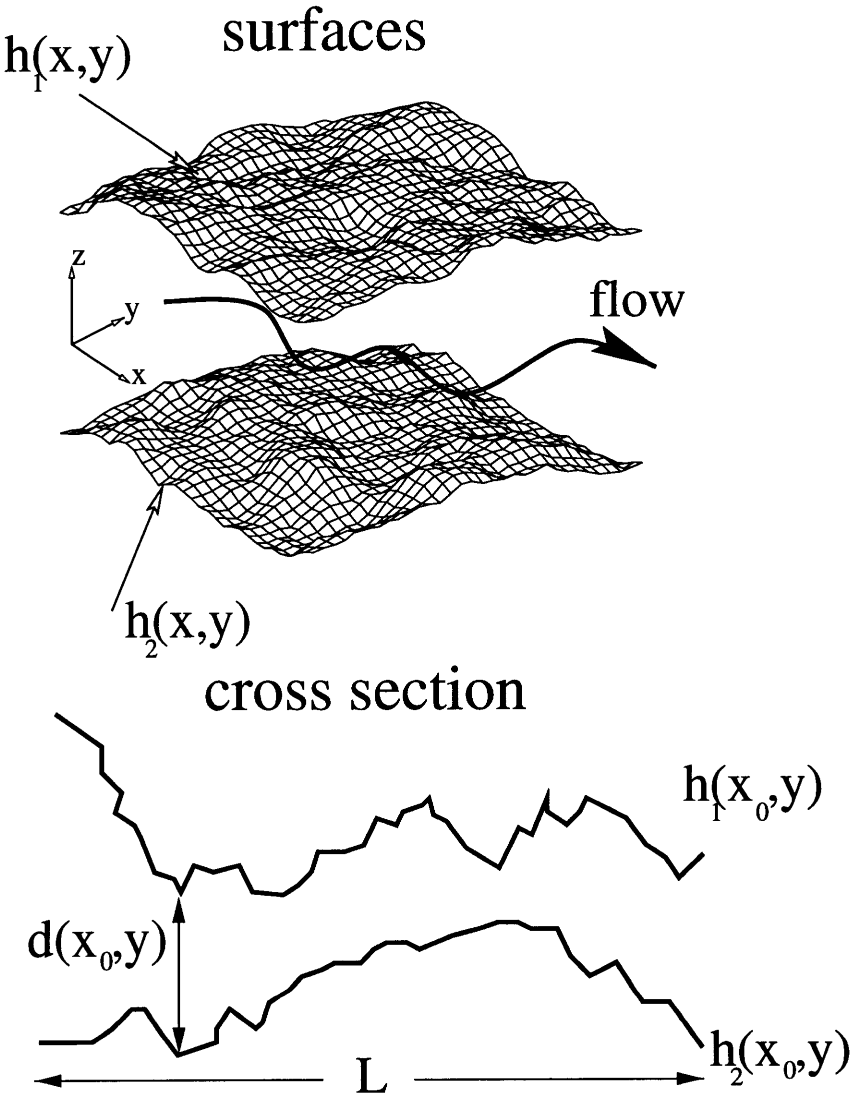

Figure 4-1: Topography of a fracture with self-affine channel walls $h_1(x, y)$ and $h_2(x, y)$ and variable aperture $d(x, y)$. The length of the fracture is L.

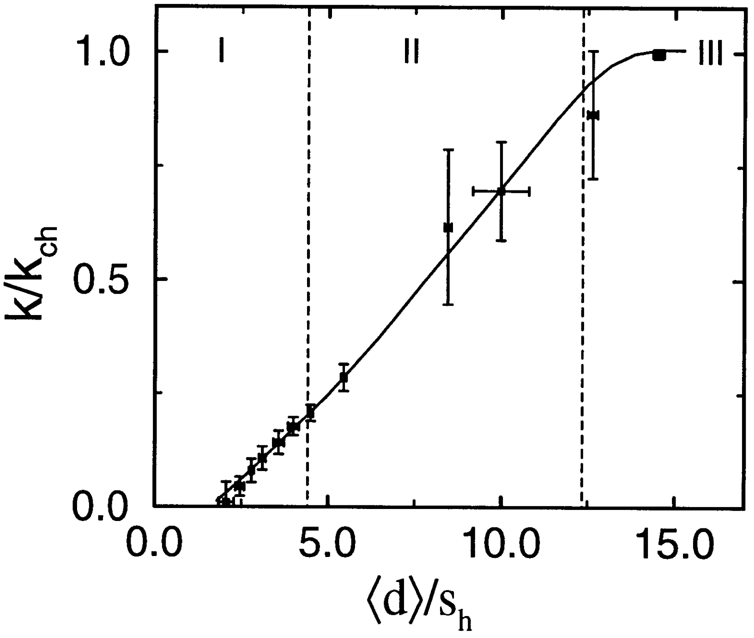

Figure 4-2: Scaled permeability k/k_{ch} versus the scaled aperture $\langle d \rangle / s_h$. The dotted line shows the trend of the data. Three different ranges of the mean apertures are differentiated and indicated with roman numbers. The dashed vertical lines are at the boundaries of each range. The flow dynamics of each region is discussed in the text below. Error bars correspond to one standard deviation.

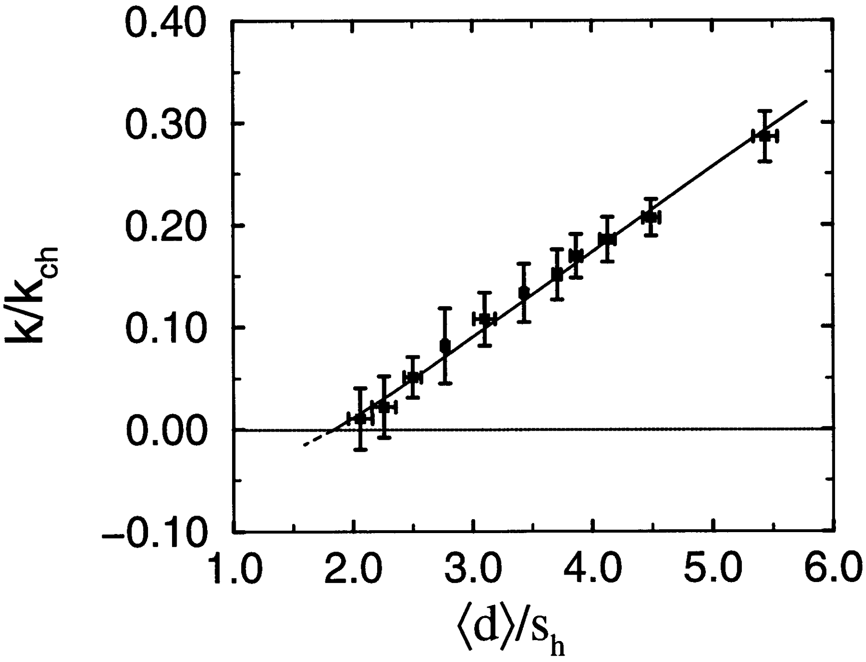

Figure 4-3: This plot shows a subset of the data set figure 3. The dotted line extrapolates the permeability data towards smaller aperture. Note that the percolation threshold of the aperture is at $d_c \approx \frac{3}{2} s_h$.

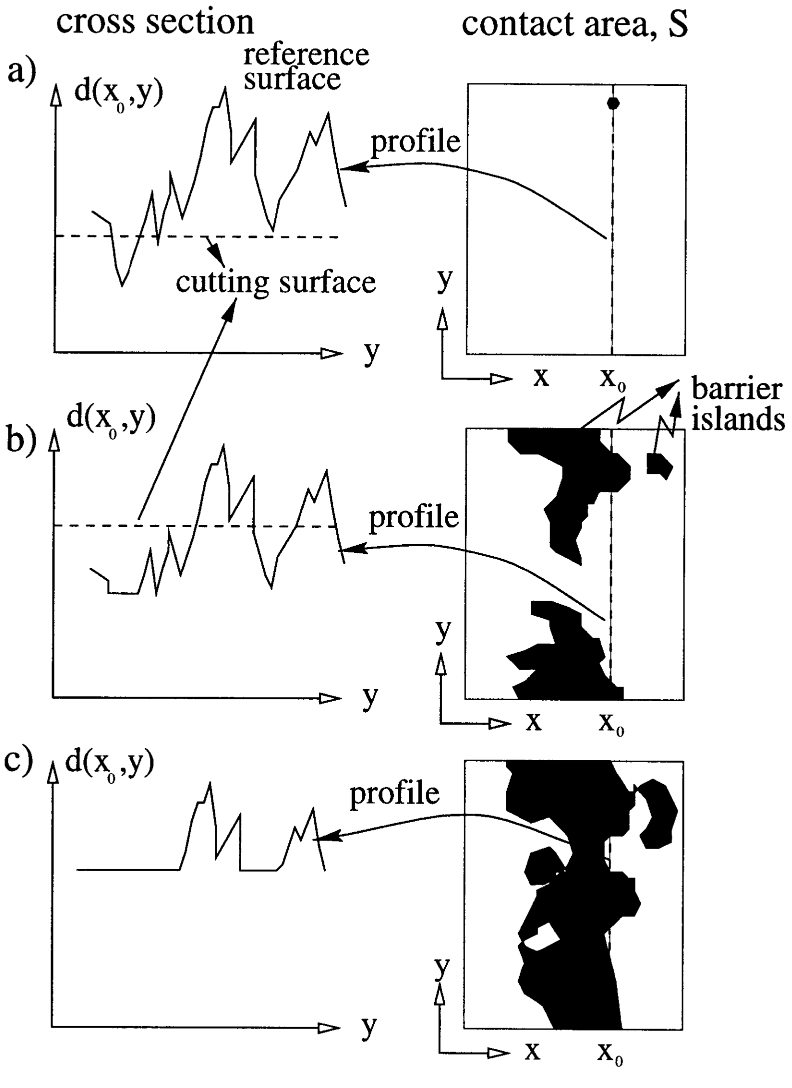

Figure 4-4: On the left-hand side are cross sections of the aperture surface and on the right-hand side the corresponding contact areas are shown. The cross sections are taken along the dashed line, $x = x_0$ of the upper right figure. For the interpretation of the figures, assume that the flow direction is from left to right or right to left. The cross section and contact area of a) is that of the reference aperture surface. The aperture in row b) is just above the percolation threshold and the fracture is closed in c), which is indicated by the large spanning barrier island. The dashed lines in the cross section indicate the position of the cutting surface, below which the surface will be cut off in the next image.

Chapter 5

Conclusions

This thesis presents both novel numerical characterizations and theoretical models of flow through highly disordered media. The central idea followed here is that the observations of the microscopic flow field itself are used to construct models of the flow.

One of the principal and novel results of this work is the conditioning of the flow by the the porosity. Specifically, the flow is strongly localized into channel-like paths for low porosities and for large porosities the flow fluctuations manifest themselves in the form of swirls. The transition between one pattern into the other is sharp, insofar as the lower moments of the flow field are concerned, such as the kurtosis or the flatness. Figure 5-1 summarizes our observations. Presently, I do not know of any possible physical mechanisms for this transition from channel to swirl flows. However, an explanation is essential for the characterization of flow through porous media.

Most of the studies used results from two dimensional simulations, since it was argued that the PDF's are similar. However, for completeness it would desirable to extend this study to 3D flow studies and it would be interesting to find out what the critical values of the porosity are.

Motivated by these observations on the flow statistics, I have constructed a simple phenomenological interim model for flow in tight porous media. In this model, the flow through the entire porous media is represented by a single channel with leaky,

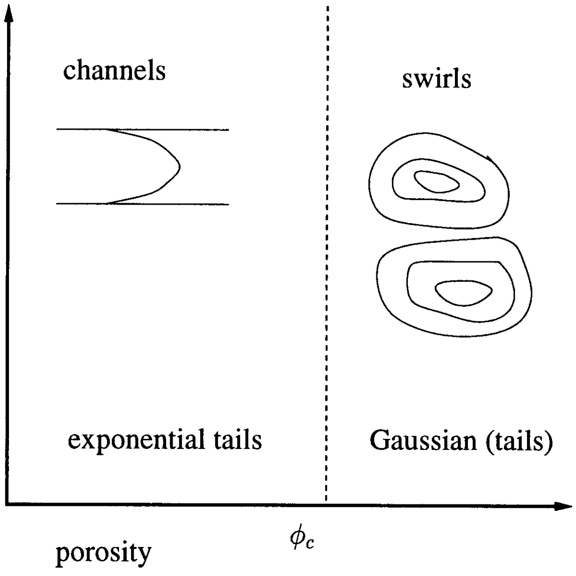

Figure 5-1: Cartoon that summarizes some of the main results of chapter 2 and chapter 3: The velocity fluctuations of flow through low porosity media are organized into localized, channel-like patterns with exponentially decaying velocity PDF's, whereas the velocity fluctuations in high porosity media are in the form of swirls with Gaussian decaying velocity PDF's. This transition is sharp and occurs at a critical porosity $\phi = \phi_c$.

slowly modulating walls. With this model the probability distribution of the velocity can be explained. One application of applying this model would be to obtain better estimates of bulk transport properties. To estimate the permeability we note that once the typical length scale $l = \alpha^{-1}$ of the channel is known and the number of channels per unit area is known, a prediction of the permeability k could be $k \propto nl^2/12$ in two dimensions. Such an expression, however, must be supplemented by an additional factor that represents an effective slip due to leakage [9, 50].

Perhaps the most important application of the leaky channel model lies in the field of hydrodynamic dispersion [49, 29]. Obviously, the leakage of the channel model is an essential feature of the dispersion of a passive scalar field. Precisely how to make this connection, however, remains a subject for future research.

The phenomenology for high porosity media comprised of fixed particles, as mentioned before, is entirely different. Because of this, there are different explanations for both porosity ranges. It is found that Brinkman's model provides a reasonable estimate for the characteristic size of the swirls. By means of a scaling argument, I have showed that the swirl size depends on the solid fraction η in nearly the same way as the average particle distance does. The power-law dependence of the amplitude on the solid fraction, however, remains unexplained and need to be addressed. This solid fraction dependence can potentially give insight regarding the aforementioned transition in the flow phenomenology.

In this thesis, I used isotropic, homogeneous random porous media. These are, however, very simple random media. An additional complexity can be introduced by including spatial correlations, which most likely will have a strong impact on the nature of the velocity fluctuations. As expected, the effects on the flow by these spatial correlations in the medium is interesting for various reasons. For example, it could give insight into the processes that form porous media, such as the formation of sedimentary rocks.

Permeability measurements for flow through a rough walled channel showed that an equivalent plane channel model overestimates the permeability. For the case of tight fractures, I have presented a theory which predicts power-law behavior of the permeability with the fracture length in cases of almost closed fractures. Clearly, this power-law dependency need to be verified. To do so numerically requires, however, (too) large system sizes and thus an experimental test of the scale dependence is, for the latter reason alone, preferable. Validation of the above prediction would have important consequences for permeability estimates of fracture networks.

Appendix A

Solution of stochastic channel equation

We seek solutions of the Langevin equation:

$$\frac{du(\tau)}{d\tau} = -\kappa^{-1}(\tau)u(\tau) + f(\tau). \tag{A.1}$$

For convenience, we have substituted u for $\hat{u}$. We assume that the f and κ are uncorrelated, such that conditions (2.20)-(2.22) hold. We will construct a PDF of u by determining all its moments. We follow the analysis of Deutsch [19].

The general solution of equation (A.1) is

$$u(\tau) = A(\tau)e^{-\int_0^t \kappa^{-1}(\tau)\,d\tau}, \tag{A.2}$$

where A can be determined from an initial condition. We assume that there exists a time for which $u = 0$. For convenience, we take the velocity $u = 0$ for $t \to -\infty$ and assume that solution is stationary for $t \geq 0$, that is $\langle u(0)^n \rangle = \langle u(t)^n \rangle$ for $t \geq 0$. Substitution of equation (A.2) in equation (A.1) yields a differential equation for A. Its solution is

$$A = \int_{-\infty}^{t} f(s)e^{-\int_0^s \kappa^{-1}(\tau)\,d\tau}\,ds. \tag{A.3}$$

Changing the variable $s \to -s$ and observing that $f(s) = f(-s)$ in (A.3) yields with

(A.2) for the stationary velocity $u(0)$,

$$u(0) = \int_0^\infty ds\; f(s) \exp\left[-\int^s d\tau \kappa^{-1}(\tau)\right]. \tag{A.4}$$

The odd moments of the velocity field are given by

$$\begin{aligned}\langle u^{2n+1}(0)\rangle = \int_0^\infty \cdots \int_0^\infty \left\langle \exp\left[-\sum_{i=1}^{2n+1} \int_0^{s_i} \kappa^{-1}(\tau)\, d\tau\right]\right\rangle \\ \times \langle f(s_1)\cdots f(s_{2n+1})\rangle\, ds_1 \cdots ds_{2n+1} = 0.\end{aligned} \tag{A.5}$$

Here, we note that odd products of normal Gaussian processes κ are zero. Hence it suffices to consider even moments only. For the even moments of the velocity field we thus find that

$$\begin{aligned}\langle u^{2n}(0)\rangle = \int_0^\infty \cdots \int_0^\infty \left\langle \exp\left[-\sum_{i=1}^{2n} \int_0^{s_i} -\kappa^{-1}(\tau)\, d\tau\right]\right\rangle \\ \times \langle f(s_1)\cdots f(s_{2n})\rangle\, ds_1 \cdots ds_{2n}\end{aligned} \tag{A.6}$$

Recall that we have taken f to be Gaussian white noise. This allows us to apply Wick's theorem [25] to the right hand side of (A.6). We thus can write for (A.6)

$$\begin{aligned}\langle u^{2n}(0)\rangle &= \frac{(2n)!}{2^n n!} \int_0^\infty \cdots \int_0^\infty \left\langle \exp\left[-\sum_{i=1}^{2n} \int_0^{s_i} -\kappa^{-1}(\tau)\, d\tau\right]\right\rangle \\ &\quad \times \delta(s_1 - s_{n+1}) \cdots \delta(s_n - s_{2n})\, ds_1 \cdots ds_{2n} \\ &= \frac{(2n)!}{2^n n!} \int_0^\infty \cdots \int_0^\infty \left\langle \exp\left[-2\sum_{i=1}^{n} \int_0^{s_i} -\kappa^{-1}(\tau)\, d\tau\right]\right\rangle ds_1 \cdots ds_n\end{aligned} \tag{A.7}$$

Once all the moments (A.7) are known, the PDF for u and thus of the entire flow is known. Here, the moments are evaluated by the introduction of Lyapunov exponents. In doing so, it is advantageous to introduce the change of variables

$$\begin{cases} s_{i+1} - s_i & \text{if } i < n, \\ s_n & \text{if } i = n, \end{cases} \tag{A.8}$$

where we define that $s_{i+1} > s_i$. Substitution of (??) into (A.7) yields

$$\langle u^{2n}(0)\rangle = \frac{(2n)!}{2^n}\prod_{i=1}^{n}\left\{\int_0^\infty \left\langle \exp\left[-2i\int_0^{\Delta_i}\kappa^{-1}(\tau)\,d\tau\right]\right\rangle d\Delta_i\right\}. \tag{A.9}$$

The kernels in the latter equation (A.9) can be identified as the generalized Lyapunov exponents [10] L,

$$\left\langle \exp\left[-2i\int_0^{\Delta_i} -\kappa^{-1}(\tau)\,d\tau\right]\right\rangle = e^{L(\Delta_i)\,2i}. \tag{A.10}$$

Then equation (A.9) becomes

$$\langle u^{2n}(0)\rangle = \frac{(2n)!}{2^n}\prod_{i=1}^{n}\left\{\int_0^\infty e^{L(\Delta_i)\,2i}\,d\Delta_i\right\}. \tag{A.11}$$

For the integration of (A.9) we use the property that $L(\Delta_i)$ is always negative. This is a direct consequence of the fact that the permeability $k(\tau)$ is always positive and thus $-\kappa^{-1}$ is always negative. Since $\lim_{\Delta_i\to\infty} e^{L(2i)\Delta_i} \to 0$, integration of equation (A.11) yields

$$\langle u^{2n}(0)\rangle = (2n)!\prod_{i=1}^{n}\frac{-1}{L(2i)}. \tag{A.12}$$

Obviously, if we know the Lyapunov coefficients $L(2n)$ then we know all the moments of the velocity field u and hence we are able to obtain the PDF for u. Deutsch [19] used stability arguments to describe the functional form L for large velocities. He then showed that equation (A.12) yields the desired equation (2.7),

$$P_u(u) \propto \exp\left[-\beta u^{\xi}\right], \tag{A.13}$$

where $1 \le \xi \le 2$ and u is large.

Bibliography

[1] D. J. Adams and A. J. Matheson. Computation of dense random packing of hard spheres. *J. Chem. Physics*, 56:1989–1994, 1972.

[2] P. Adler. *Porous media: geometry and transports.* Butterworth/Heinemann, 1992.

[3] J. S. Andrade, M. P. Almeida, J. Mendes Filho, S. Havlin, B. Suki, and H. E. Stanley. Fluid flow though porous media: The role of stagnant zones. *Phys. Rev. Lett.*, 79:3901–3904, 1997.

[4] F. M. Auzerais, J. Dunsmuir, B. Ferréol, N. Martys, J. Olson, T. S. Ramakrishnan, D. H. Rothman, and L. M. Schwartz. Transport in sandstone: a study based on three-dimensional microtomography. *Geophys. Res. Lett.*, 23:705–708, 1996.

[5] G. K. Batchelor. *The theory of homogenous turbulence.* Cambridge University Press, 1953.

[6] G. K. Batchelor. *An Introduction to Fluid Dynamics.* Cambridge University Press, Cambridge, 1967.

[7] G. K. Batchelor. Sedimentation in a dilute dispersion of spheres. *J. Fluid Mech.*, 52:245–268, 1972.

[8] J. Bear. *Dynamics of Fluids in Porous Media.* Dover Publications, New York, 1972.

[9] G. S. Beavers and D. D. Joseph. Boundary conditions at a naturally permeable wall. *F. Fluid Mech.*, 30:197–207, 1967.

[10] R. Benzi, G. Paladin, G. Parisi, and A. Vulpiani. Characterisation of intermittency in chaotic systems. *J. Phys. A*, 18:2157–2165, 1985.

[11] J. G. Berryman and G. W. Milton. Bounds on fluid permeability for viscous flow through porous media. *J. Chem. Phys*, 82:1459–1467, 1985.

[12] H. C. Brinkman. A calculation of the viscous force exerted by a flowing fluid on a dense swarm of particles. *Appl. Sci. Res.*, A1:27–34, 1947.

[13] S. R. Brown. Fluid flow through rock joints: The effect of surface roughness. *J. Geophys. Res.*, 92:1337–1347, 1987.

[14] S. R. Brown. Simple mathematical model of a rough fracture. *J. Geophys. Res.*, 100, 1997.

[15] S. R. Brown and C. H. Scholz. Closure of random elastic surfaces in contact. *J. Geol. Res.*, 90:5531–5544, 1985.

[16] J. Buckles, R. Hazlett, S. Chen, K. Eggert, D. Grunau, and W. Soll. Toward improved prediction of reservoir flow performance. *Los Alamos Science*, 22:112–121, 1994.

[17] A. Cancelliere, C. Chang, E. Foti, D. H. Rothman, and S. Succi. The permeability of a random medium: Comparison of simulation with theory. *Physics of Fluids A*, 2:2085–2088, 1990.

[18] S. Childress. Viscous flow past a random array of spheres. *J. Chem. Phys.*, 56:2527–2539, 1972.

[19] J. Deutsch. Probability distributions for one-component equations with multiplicative noise. *Physica A*, 208:433–444, 1994.

[20] D. d'Humières and R. Cornubert. Flow past a symmetric back-facing step using lattice-Boltzmann equations. preprint, 1993.

[21] B. Ferréol and D. H. Rothman. Lattice-Boltzmann simulations of flow through Fontainebleau sandstone. *Transport in Porous Media, in press*, 1995.

[22] U. Frisch. *Turbulence: the legacy of A.N. Kolmogorov.* Cambridge University Press, 1995.

[23] I. Ginzbourg and P. M. Adler. Boundary flow condition analysis for the three-dimensional lattice-Boltzmann model. *J. Physique II France*, 4:191–214, 1994.

[24] I. Ginzbourg and D. d'Humières. Local second order boundary method for lattice Boltzmann models. *preprint*, 1995.

[25] N. Goldenfield. *Lectures on phase transitions and the renormalization group.* Addison-Wesley Publishing Company, 1992.

[26] A. Heijs and C. Lowe. Numerical evaluation of the permeability and the Kozeny constant for two types of porous media. *Phys. Rev. E*, 51:4346–4352, 1995.

[27] I. D. Howell. Drag due to the motion of Newtonian fluid through a sparse random array of small fixed rigid objects. *J. Fluid Mech.*, 64:449–475, 1974.

[28] M. B. Isichenko. Percolation, statistical topography, and transport in random media. *Rev. Mod. Phys.*, 64:961, 1992.

[29] D. L. Koch and J. F. Brady. Dispersion in fixed beds. *J. Fluid Mech.*, 154:399–427, 1985.

[30] A. Koponen, D. Kandhai, E. Hell, M. Alava, A. Hoekstra, M. Kataja, K. Niskanen, P. Sloot, and J. Timonen. Permeability of three-dimensional random fiber webs. *Phys. Rev. Lett.*, 80:716–719, 1998.

[31] Y. Kutsovsky, L. Scriven, H. Davis, and B. Hammer. NMR imaging of velocity profiles and velocity distributions in bead packs. *Phys. Fluids*, 8:863, 1995.

[32] A. J. C. Ladd. Numerical simulations of particulate suspensions via a discretized Boltzmann equation. Part 1. Theoretical foundation. *J. Fluid Mech.*, 271:285–310, 1994.

[33] L. Lebon, L. Oger, J. Leblond, J. P. Hulin, N. S. Martys, and L. M. Schwartz. Pulsed gradient NMR measurements and numerical simulation of flow velocity distribution in sphere packings. *Phys. Fluid*, 8:293–301, 1995.

[34] R. Lemaitre and P. M. Adler. Fractal porous media IV: Three-dimensional Stokes flow through random media. *Transport in Porous Media*, pages 325–340, 1990.

[35] T. S. Lundgren. Slow flow through stationary random beds and suspensions of spheres. *J. Fluid Mech.*, 51:273–299, 1972.

[36] R. S. Maier, D. M. Kroll, Y. E. Kutsovsky, H. T. Davis, and R. S. Bernard. Simulation of flow through bead packs using the lattice Boltzmann method. *Phys. Fluids*, 10:60–74, 1998.

[37] A. S. Monin and A. M. Yaglom. *Statistical fluid mechanics; mechanics of turbulence.* MIT press, 1975.

[38] V. V. Mourzenko, J. F. Thovert, and P. M. Adler. Permeability of a single fracture: Validity of the Reynolds equation. *J. Phys. II France*, 5:465–482, 1995.

[39] J. F. Olson and D. H. Rothman. Two-phase flow in sedimentary rock: simulation, transport and complexity. *J. Fluid Mech.*, 341:343–370, 1997.

[40] R. Peyret and T. D. Taylor. *Computational Methods for Fluid Flow.* Springer-Verlag, 1983.

[41] O. Pinkus and B. Sternlicht. *Theory of hydrodynamic lubrication.* McGraw-Hill, NewYork, 1961.

[42] S. Prager. Viscous flow through porous media. *Phys. Fluids*, 4:1477–1482, 1961.

[43] Y. H. Qian, D. d'Humières, and P. Lallemand. Lattice BGK models for Navier-Stokes equation. *Europhys. Lett.*, 17(6):479–484, 1992.

[44] P. C. Rem and J. A. Somers. Cellular automata on a transputer network. In R. Monaco, editor, *Discrete Kinetic Theory, Lattice-Gas Dynamics, and Foundations of Hydrodynamics*, pages 268–275. World Scientific, 1989.

[45] D. H. Rothman. Cellular-automaton fluids: A model for flow in porous media. *Geophysics*, 53:509–518, 1988.

[46] D. H. Rothman and S. Zaleski. *Lattice-gas cellular automata: Simple models of complex hydrodynamics.* Cambridge University Press, Cambridge, 1997.

[47] S. Roux, J. Schmittbuhl, J. P. Vilotte, and A. Hansen. Some physical properties of self-affine rough surfaces. *Europhys. Lett.*, 23:277–282, 1993.

[48] J. Rubinstein and S. Torquato. Flow in random porous media: mathematical formulation, variational principles, and rigorous bounds. *J. Fluid Mech.*, 206:25–46, 1989.

[49] P. G. Saffman. A theory of dispersion in porous media. *J. Fluid Mech.*, 6:321–349, 1959.

[50] P. G. Saffman. On the boundary condition at the surface of a porous medium. *Stud. Appl. Math*, pages 93–101, 1971.

[51] P. G. Saffman. On the settling speed of free and fixed suspensions. *Studies in Applied Mathematics*, LII:115–127, 1973.

[52] A. S. Sangani and C. Yao. Transport process in random arrays of cylinders. II. viscous flow. *Phys. Fluids*, 31:2435–2444, 1988.

[53] A. E. Scheidegger. *The Physics of Flow Through Porous Media, 3rd ed.* University of Toronto Press, Toronto, 1974.

[54] J. Schmittbuhl, , J.P. Vilotte, and S. Roux. Percolation through self-affine surfaces. *J. Phys. A.*, 26:6115–6133, 1993.

[55] J. Schmittbuhl, F. Schmit, and C. Scholtz. Scaling invariance of crack surfaces. *J. Geophys. Res.*, 100:5933–5973, 1995.

[56] G. D. Scott. The packing of spheres. *Nature*, 188:908–909, 1960.

[57] P. N. Segré, E. Herbolzheimer, and P. M. Chaikin. Long-range correlations in sedimentation. *Phys. Rev. Lett.*, 13:2574–2577, 1997.

[58] W. Soll, S. Chen, K. Eggert, D. Grunau, and D. Janecky. Application of the lattice-Boltzmann/lattice gas technique to multi-fluid flow in porous media. In A. Peters, editor, *Computational methods in water resources X*, pages 991–999. Kluwer Academic Publishers, 1994.

[59] P. Spanne, J. F. Thovert, C. J. Jacquin, W. B. Lindquist, K. W. Jones, and P. M. Adler. Synchrotron computed microtomography of porous media: topology and transport. *Phys. Rev. Lett.*, 73:2001–2004, 1994.

[60] H. E. Stanley. *Introduction to Phase Transitions and Critical Phenomena.* Dover Publications, New York, 1971.

[61] D. Stauffer and A. Aharony. *Introduction to percolation theory.* Taylor & Francis, 1992.

[62] D. L. Turcotte. *Fractals and chaos in geology and geophysics.* Cambridge University Press, Cambridge, 1992.

[63] O. van Genabeek and D. H. Rothman. Macrocopic manifestations of microscopic flows through porous media: Phenomenology from simulation. *Annu. Rev. Earth Planet. Sci.*, 24:63–87, 1996.

[64] R. F. Voss. Random fractal forgeries. In R.A. Earnshaw, editor, *Fundamental algorithms for computer graphics.* Springer-Verlag, Berlin, 1985.

[65] H. L. Weissberg and S. Prager. Viscous flow throught porous media. III. Upper bounds on the permeability for a simple random geometry. *Phys. Fluids*, 12:2958–2965, 1970.

[66] R. W. Zimmerman and G.S. Bodvarsson. Hydraulic conductivity of rock fractures. *Transport in Porous Media*, 23:1–30, 1996.

[illegible]